International Communications in Heat and Mass Transfer 151 (2024) 107207

Contents lists available at ScienceDirect

International Communications in Heat and Mass Transfer

journal homepage: www.elsevier.com/locate/ichmt

Dual-sided melting of a one-dimensional composite wall comprising two distinct phase change material (PCM) layers

Emad Hasrati, Ankur Jain *

Mechanical and Aerospace Engineering Department, University of Texas at Arlington, Arlington, TX, USA

ARTICLE INFO

Keywords:
Composite phase change materials
Melting and solidification
Stefan problems
Multilayer wall
Moving boundary problems

ABSTRACT

Past literature on theoretical modeling of solid-liquid phase change heat transfer mostly addresses a single phase change material (PCM), whereas, a series combination of two or more PCMs is often used in practical applications. This work presents an approximate analytical model for the melting/freezing of a one-dimensional composite of two PCMs being heated/cooled from both ends. It is shown that up to three phase change fronts may simultaneously exist in this problem. In addition to direct melting/freezing from the respective walls, it is shown that each PCM may also melt/freeze due to heat transfer through the other PCM. Using a quasi-stationary assumption, temperature field during the multi-stage phase change process is approximated by solving a multilayer transient thermal conduction problem using eigenfunction expansion. Good agreement with numerical simulations, and with the Stefan solution for a special case is demonstrated. The impact of key non-dimensional parameters on performance metrics including total time for phase change is determined. A quantitative prediction of conditions leading to the thermodynamically favorable situation of simultaneous completion of phase change of two commonly used PCMs is carried out. This work improves the theoretical understanding of phase change in composite PCMs, leading to optimization of practical thermal systems.

1. Introduction

Melting and solidification are important heat transfer processes that occur commonly in thermal management and energy conversion systems [1–3]. Understanding the fundamental nature of melting and solidification is critical for designing and optimizing the performance of such systems. For example, phase change materials (PCMs) have been investigated for thermal management of Li-ion cells [4], for which, understanding the parameters that govern propagation of the melting front is important for addressing performance-vs-weight trade-offs.

Phase change heat transfer processes are usually modeled on the basis of a propagating phase change front driven by an externally applied boundary condition [1]. The simplest of such problems – one-dimensional phase change due to an isothermal boundary condition – has a well-known analytical solution [1,5]. However, most realistic phase change problems, such as those with multi-dimensional geometry [6], encapsulant layer [7,8], phase change over a temperature range [1] and temperature-dependent thermal properties [9] are non-linear in nature, and lack an exact solution. Therefore, a number of approximate techniques such as quasi-stationary [2], perturbation [10,11] and integral methods [12] have been developed. An extension of the quasi-stationary technique involves solving for the transient temperature distribution in the newly formed phase and using conservation of energy at the interface to determine the rate of propagation of the phase change front [7]. This technique has been used to solve phase change problems with internal heat generation [13], time-dependent boundary conditions [14] and in encapsulated PCMs [7,8,15]. Such techniques typically offer reasonably low error when the phase change front moves relatively slowly, i.e., for small values of the Stefan number. In addition to such analytical techniques, numerical calculations, mostly based on the enthalpy method [16] or the variable timestep method [17] have also been developed.

Most of the literature on theoretical modeling of melting and solidification processes addresses a single PCM scenario. However, several practical applications involve the use of more than one PCM, often arranged as a composite stack, such as the one shown in Fig. 1. Based on exergy analysis, it has been shown [18] that the use of two or more PCMs in series may be thermodynamically favorable over a single PCM due to a reduction in irreversibility. The impact of melting temperatures of the stacked PCMs on thermodynamic performance has been presented [19]. Optimization of the charge-discharge process using finite-element

* Corresponding author at: 500 W First St, Rm 211, Arlington, TX 76019, USA.
E-mail address: jaina@uta.edu (A. Jain).

https://doi.org/10.1016/j.icheatmasstransfer.2023.107207

Nomenclature

C_p	heat capacity ($Jkg^{-1}\ K^{-1}$)
k	thermal conductivity ($Wm^{-1}\ K^{-1}$)
$\bar{k}_2$	ratio of thermal conductivities
L	layer thickness (m)
$\mathscr{L}$	latent heat of phase change (Jkg^{-1})
Ste	Stefan number
t	time (s)
T	temperature (K)
x	spatial coordinate (m)
α	thermal diffusivity (m^2s^{-1})
$\bar{\alpha}_2$	ratio of thermal diffusivities
γ	non-dimensional interface location
ϕ	non-dimensional melting temperature of higher-melting layer
τ	non-dimensional time
θ	non-dimensional temperature
ξ	non-dimensional spatial coordinate

Subscripts

A, B, C	stages
f	phase change temperature
w	wall
LS	phase change front location
$1, 2$	layer number

modeling has been carried out [20]. The problem of sizing of a two-PCM energy storage unit to ensure simultaneous completion of phase change in both PCMs has been presented [21]. A latent heat energy storage system based on a cascade of PCMs has been designed [22]. Theoretical analysis of heat transfer in a bank of cylinders containing three different PCMs has been reported [23]. Melting of multiple PCMs arranged in a heat exchanger has been analyzed through numerical simulations [24]. A theoretical model for phase change in a composite PCM has been reported [25]. The effect of series/parallel arrangement of multiple PCMs on energy storage performance has been evaluated numerically [26]. Related experimental work includes measurements of phase change heat transfer in a three-PCM stack [27], measurement of charging/discharging of a multi-PCM cylinder [28], heat transfer measurements on a cascaded PCM arrangement for solar energy storage [29], experimental characterization of thermal management of an electronics device using a three-PCM composite [30] and measurement of enhanced charging/discharging of a latent heat energy storage unit by the use of three PCMs in series [31]. While much of the literature summarized above focuses on the thermodynamics of composite PCMs and overall heat exchanger calculations, there is a lack of sufficient work on heat transfer modeling to predict the propagation of the melting fronts in a composite PCM. For example, while past work predicts that simultaneous completion of phase change in each PCM is thermodynamically favorable [18], there is a lack of work on determining conditions in which such simultaneous completion of phase change will occur.

This is an important research gap because while the melting of a single PCM can be modeled quite easily using tools referenced above, the presence of two or more PCMs results in significant additional complexity. For example, more than one phase change front may propagate simultaneously during the melting/solidification of two PCMs connected in series with each other. In addition to direct melting due to heat transfer from the boundaries, melting of one PCM may also be driven by heat transfer through the other PCM. In such a case, a number of additional variables govern the nature of melting propagation, including the two melting temperatures relative to the imposed boundary condition, thermal properties of the two PCMs relative to each other, including latent heats and thermal diffusivities, as well as the order in which the PCMs are arranged. An analytical solution for this problem is critically needed in order to understand the impact of these variables on the melting process. An important question of practical interest is the optimal design of the composite PCM to ensure that both PCMs finish melting simultaneously, so that the latent thermal energy storage potential of both PCMs is fully utilized.

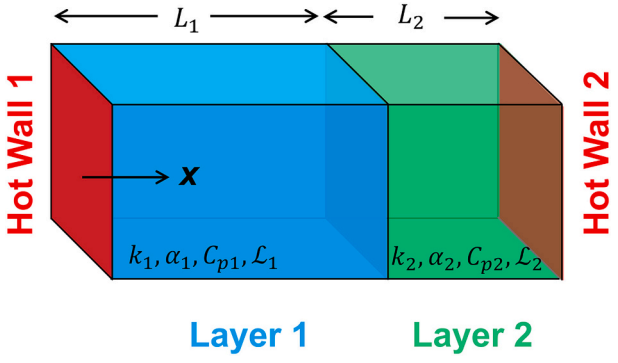

Fig. 1. Schematic of the problem under consideration: a stack of two phase change materials with dissimilar thermal properties exposed to heating by constant temperature walls from both ends.

Unfortunately, most of the available work on melting of a composite PCM is based on numerical simulations, as summarized above, and is not general enough to provide insights into the fundamental nature of the problem, such as the key non-dimensional parameters that govern the melting process. In recent work [32], the problem of melting of a stack of two PCMs arranged in series due to a high temperature imposed on one end of the stack was investigated. However, this work only considered melting driven from one end, whereas, in realistic problems, the composite PCM may be subjected to heating from both sides, such as shown in Fig. 1. When heated from both sides, the two PCMs may melt in series or parallel, and more than one melting fronts may be present. The interaction between the two PCMs in this case is quite complex, and can not be obtained from trivial extension of past work. Identification of key non-dimensional parameters and their impact on phase change progression in a dual-sided melting problem requires careful consideration of heat transfer in both PCMs and energy conservation applied simultaneously to multiple melting fronts. The current lack of such work hinders further optimization of two-PCM composites that are predicted to offer reduced thermodynamic irreversibility and improved performance compared to a single PCM.

This work presents an approximate analytical solution of the problem of dual-sided melting of a two-PCM composite wall using the eigenfunction expansion technique. A systematic analysis of all possible stages during the melting process, including multiple simultaneous melting fronts is presented. A key practical question of the design of the composite to ensure simultaneous completion of melting of both layers is addressed. The role of key non-dimensional parameters in this problem is discussed. In contrast with recent work on thermal modeling of two-PCM phase change problems, the novelty of the present work is that it considers the realistic scenario of melting from both ends, which is not solvable using straightforward extension of past work. By solving a problem of much relevance to practical multi-PCM systems, this work contributes towards a better understanding of the design and optimization of such systems.

2. Problem definition

The problem of interest comprises a composite wall of two PCMs arranged in series, as shown in Fig. 1. The thicknesses of the two PCMs in the x direction shown are L_1 and L_2, respectively. PCM sizes in the other directions are assumed to be large enough and/or the other directions are assumed to be insulated, so that the problem can be considered one-dimensional in the x direction. The melting temperature of the two PCMs are denoted by $T_{f,1}$ and $T_{f,2}$, respectively. Phase change in both PCMs is assumed to occur at a single temperature, as is typical for pure materials, rather than over a temperature range, such as in alloys and mixtures. Melting is simultaneously driven from both left and right walls that are assumed to be maintained at constant temperatures $T_{w,1}$ and $T_{w,2}$, respectively. Without loss of generality, the left-side PCM is assumed to have the lower melting temperature, i.e., $T_{f,1} < T_{f,2}$. The entire PCM stack is assumed to be initially at the lower of the two melting temperatures, i.e., at $T_{f,1}$. Thermal diffusivity, thermal conductivity, heat capacity and latent heat are denoted by α, k, C_p and $\mathscr{L}$, respectively, with a subscript to indicate one of the two PCMs. All thermal properties are assumed to be independent of temperature. Convection in the newly formed fluid phase is ignored, based on the assumption of a sufficiently small Rayleigh number due to a small range of temperature change. While analysis is presented here in the context of melting, the opposite problem of freezing can be analyzed similarly.

Since both PCMs are exposed to wall temperatures greater than their respective melting temperature, therefore, starting at $t = 0$, both PCMs begin to melt. As time passes, the two melting fronts continue to propagate inwards, starting from the left and right walls, respectively. These melting fronts that propagate due to heat transfer directly from a hot wall are referred to as primary melting fronts. Due to the distinct properties of the two PCMs, the propagation of the two melting fronts is not completely independent of each other in this problem. Further, it is possible that, under certain conditions, additional melting fronts may be induced in one or both layers, so that in addition to melting caused by heat transfer directly from the wall, a layer may also melt from the other side due to heat transferred to it through the other layer. A melting front in a layer due to heat transfer through the other layer is referred to as a secondary melting front. Due to the complicated dynamics of these processes, it is important to systematically model the coupled phase change processes in the two PCMs, and track both primary and secondary melting fronts.

Fig. 2 schematically shows the overall progression of the melting process, based on which, it is broken down into multiple sequential stages. Starting at $t = 0$, both layers begin to melt simultaneously, which is referred to as Stage A. Subsequently, depending on which of the two layers finishes melting first, two distinct Cases may occur, as shown in Fig. 2. In Case I, layer 2 finishes melting first and layer 1 finishes melting at a later time in Stage B. Qualitatively, this may occur if layer 2 is relatively thin, wall temperature at the end of layer 2 is relatively large and/or layer 2 material has relatively low latent heat of phase change. In contrast, in Case II, layer 1 finishes melting first, while layer 2 is only partially melted at the time of completion of melting of layer 1. Subsequently, layer 2 continues to melt during Stage B. Under certain conditions, a secondary melting front may also occur in layer 2, which is referred to as Stage C. Detailed mathematical modeling of these two Cases and various Stages therein are presented separately in the following sub-sections.

2.1. Case I: Layer 2 finishes melting first

As shown in Fig. 2, the first stage of the melting process, referred to as Stage A comprises simultaneous melting of both layers. While both layers 1 and 2 begin to melt due to high temperature at their respective ends, in addition, because layer 1 has the lower melting temperature, therefore, some heat transfer through the melted and unmelted regions of layer 2 also causes melting of layer 1 due to a secondary melting front. This melting front starts from the inter-layer interface and propagates left-wards in layer 1, as shown in the Stage A schematic in Fig. 2.

Case I represents the scenario in which layer 2 finishes melting first at the end of Stage A. Subsequently, in Stage B, layer 1 continues to melt, while there is sensible heating in layer 2 as well. Eventually, both fronts in layer 1 unite, indicating the completion of melting.

In order to systematically analyze thermal conduction and phase change in each of the Stages described above, it is helpful to first carry out a non-dimensionalization of the problem as follows: $\xi = \frac{x}{L_1+L_2}$, $\tau = \frac{\alpha_1 t}{(L_1+L_2)^2}$, $\theta_i = \frac{T_i - T_{f,1}}{T_{w,1} - T_{f,1}}$, $Ste_i = \frac{C_{p,i}(T_{w,1} - T_{f,1})}{\mathscr{L}_i}$, $\xi_{LS,i} = \frac{x_{LS,i}}{L_1+L_2}$, $\phi_2 = \frac{T_{f,2} - T_{f,1}}{T_{w,1} - T_{f,1}}$, $\gamma = \frac{L_1}{L_1+L_2}$, $\bar{\alpha}_2 = \frac{\alpha_2}{\alpha_1}$, $\bar{k}_2 = \frac{k_2}{k_1}$, $\theta_{w,i} = \frac{T_{w,i} - T_{f,1}}{T_{w,1} - T_{f,1}}$, $(i = 1, 2)$.

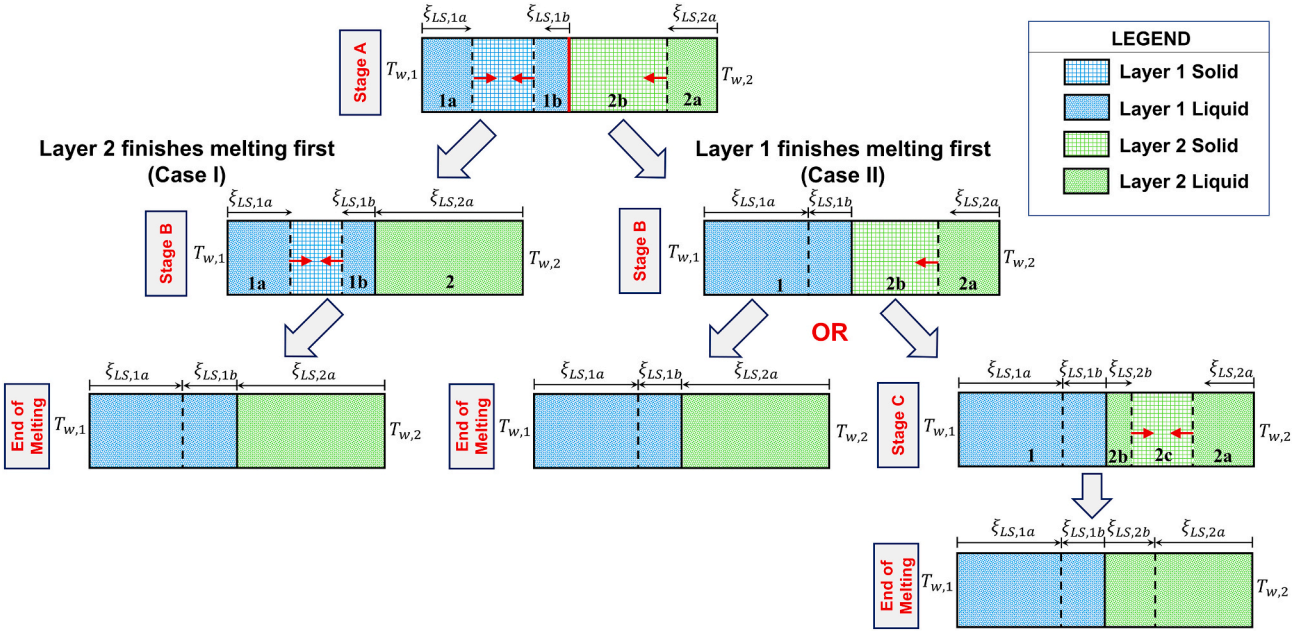

Fig. 2. Schematics showing the general progression of melting process in the two-PCM stack, as well as Cases I and II, and Stages within, based on which, the analysis in this work is organized.

Note that definitions of both Stefan numbers use the left wall temperature. Therefore, the two Stefan numbers represent the effect of thermal properties C_p and $\mathscr{L}$ of each layer, whereas the impact of the wall temperature is represented by the non-dimensional wall temperature $\theta_{w,i}$. Further, note that $x_{LS,i}$ $(i = 1, 2)$ represents the location of the melting front in each layer. Subscripts a and b are also added in order to denote primary and secondary melting fronts. For layers 1 and 2, primary melting front locations are measured from the left and right walls, respectively, and propagate rightwards and leftwards, respectively. In contrast, secondary melting front locations are measured from the interface between layers, and travel leftwards and rightwards, respectively.

Based on such non-dimensionalization, the energy conservation equations that govern the temperature field and melting propagation are written and solved for each Stage in sub-sections below. The method of eigenfunction expansion is used [7,8,13,15]. As an approximation, temperature field in the melted region of any layer at a given time is assumed to be given by the solution of the transient energy conservation equation in that layer, subject to appropriate boundary conditions along with a fixed (i.e., quasi-stationary) melting front at that time. Subsequently, the rate of melting front propagation is determined by an appropriate energy balance at the interface, which connects the rate of propagation of the melting front to the instantaneous temperature gradient at the interface. This approximate technique has been used extensively in the recent past, especially to solve multi-layer phase change problems [7,8,13,15]. While inherently approximate, this method has been shown to offer lower error than the quasi-stationary method [7,8], which effectively ignores all transient phenomena in the temperature distribution [2]. The following sub-sections describe the two Stages that occur during melting of the two-PCM composite when Case I applies.

2.1.1. Stage A: Simultaneous melting of both layers

During Stage A, melting occurs in both layers 1 and 2. While layer 2 melts only left-wards, layer 1, by virtue of being the lower-melting material, has two simultaneous melting fronts – a primary melting front that propagates right-wards starting at $x = 0$ due to heat transfer directly from the left wall, and a secondary melting front that propagates left-wards starting at $x = L_1$ due to heat transfer from the right wall through layer 2. These primary and secondary melting fronts are shown in Fig. 2.

The thermal conduction problem during Stage A comprises single-layer thermal conduction problems in the melted regions of layers 1 and layer 2 next to their respective walls, labeled 1a and 2a, respectively, along with an independent two-layer problem comprising the unmelted regions of layers 1 and 2, labeled 1b and 2b, respectively. These layers are shown schematically in Fig. 2. The governing equation for temperature distribution in layer 1a is given by,

$$\frac{\partial^2\theta_{1a}}{\partial\xi^2} = \frac{\partial\theta_{1a}}{\partial\tau} \quad (0 < \xi < \xi_{LS,1a}) \tag{1}$$

along with the following boundary conditions

$$\theta_{1a} = 1 \quad (\xi = 0) \tag{2}$$

$$\theta_{1a} = 0 \quad (\xi = \xi_{LS,1a}) \tag{3}$$

where $\xi_{LS,1a}$ refers to the primary melting front location in layer 1, as shown in Fig. 2. Note that even though $\xi_{LS,1a}$ is a function of time, based on the quasi-stationary approximation discussed above, it is being assumed to be fixed at any given time.

The melting problem described by Eqs. (1)–(3) is a standard one-dimensional Stefan problem with constant temperature boundary condition. The widely recognized analytical solution for this problem is [1],

$$\theta_{1a}(\xi,\tau) = 1 - \frac{\mathrm{erf}\left(\frac{\xi}{2\sqrt{\tau}}\right)}{\mathrm{erf}\left(\frac{\xi_{LS,1a}}{2\sqrt{\tau}}\right)} \tag{4}$$

within the region $0 < \xi < \xi_{LS,1a}$. Moreover, the location of phase change front is given by [1],

$$\xi_{LS,1a} = 2\lambda\sqrt{\tau} \tag{5}$$

where λ is the root of the equation $x\cdot\mathrm{erf}(x)\cdot\exp(x^2) = \frac{Ste_1}{\sqrt{\pi}}$ [1].

In contrast, at any given time τ, temperature fields in layer 1b for $\gamma - \xi_{LS,1b} < \xi < \gamma$ and layer 2b for $\gamma < \xi < 1 - \xi_{LS,2a}$ are governed by,

$$\frac{\partial^2\theta_{1b}}{\partial\xi^2} = \frac{\partial\theta_{1b}}{\partial\tau} \quad (\gamma - \xi_{LS,1b} < \xi < \gamma) \tag{6}$$

$$\frac{\partial^2\theta_{2b}}{\partial\xi^2} = \frac{1}{\bar{\alpha}_2}\frac{\partial\theta_{2b}}{\partial\tau} \quad (\gamma < \xi < 1 - \xi_{LS,2a}) \tag{7}$$

along with the following interface and boundary conditions,

$$\theta_{1b} = 0 \quad (\xi = \gamma - \xi_{LS,1b}) \tag{8}$$

$$\theta_{1b} = \theta_{2b} \quad (\xi = \gamma) \tag{9}$$

$$\frac{\partial\theta_{1b}}{\partial\xi} = \bar{k}_2\frac{\partial\theta_{2b}}{\partial\xi} \quad (\xi = \gamma) \tag{10}$$

$$\theta_{2b} = \phi_2 \quad (\xi = 1 - \xi_{LS,2a}) \tag{11}$$

where $\xi_{LS,1b}$ and $\xi_{LS,2a}$ refer to the secondary melting front location in layer 1 and primary melting front location in layer 2, respectively, as illustrated in Fig. 2.

This is a two-layer conduction problem with a non-homogeneous boundary condition given by Eq. (11). A standard technique to solve such a problem is to split the solution in two parts, one of which accounts for the non-homogeneity. Subsequently, an eigenfunction-based series solution is written for the second part, and the eigenvalues and various coefficients in the series are determined using the boundary conditions. Based on this process, a solution for the temperature distribution in layers 1b and 2b may be derived as follows,

$$\theta_{1b}(\xi\tau) = -\frac{\bar{k}_2\phi_2(\xi - \gamma + \xi_{LS,1b})}{\gamma + \xi_{LS,2a} - \bar{k}_2\xi_{LS,1b} - 1} + \sum_{n=1}^{\infty} c_n\big[-\tan\big(\omega_n(\gamma - \xi_{LS,1b})\big)\cos(\omega_n\xi) + \sin(\omega_n\xi)\big]\exp\big(-\omega_n^2\tau\big) \tag{12}$$

$$\theta_{2b}(\xi,\tau)=\phi_2-\frac{\phi_2\left(\xi+\xi_{LS,2a}-1\right)}{\gamma+\xi_{LS,2a}-\bar{k}_2\,\xi_{LS,1b}-1}+\sum_{n=1}^{\infty}c_n\left[\left(-\frac{\sqrt{\bar{\alpha}_2}\sin\left(\frac{\gamma\omega_n}{\sqrt{\bar{\alpha}_2}}\right)\cos\left(\omega_n\xi_{LS,1b}\right)-\bar{k}_2\cos\left(\frac{\gamma\omega_n}{\sqrt{\bar{\alpha}_2}}\right)\sin\left(\omega_n\xi_{LS,1b}\right)}{\bar{k}_2\cos\left(\omega_n\left(\gamma-\xi_{LS,1b}\right)\right)}\right)\cos\left(\frac{\omega_n}{\sqrt{\bar{\alpha}_2}}\,\xi\right)\right.$$
$$\left.+\left(\frac{\sqrt{\bar{\alpha}_2}\cos\left(\frac{\gamma\omega_n}{\sqrt{\bar{\alpha}_2}}\right)\cos\left(\omega_n\xi_{LS,1b}\right)+\bar{k}_2\sin\left(\frac{\gamma\omega_n}{\sqrt{\bar{\alpha}_2}}\right)\sin\left(\omega_n\xi_{LS,1b}\right)}{\bar{k}_2\cos\left(\omega_n\left(\gamma-\xi_{LS,1b}\right)\right)}\right)\sin\left(\frac{\omega_n}{\sqrt{\bar{\alpha}_2}}\,\xi\right)\right]\exp\left(-\omega_n^2\tau\right) \tag{13}$$

where the eigenvalues ω_n may be obtained as the roots of the following eigenequation,

$$\cos\left(\frac{\omega_n\left(\xi_{LS,2a}-1\right)}{\sqrt{\bar{\alpha}_2}}\right)\left(\bar{k}_2\cos\left(\frac{\gamma\omega_n}{\sqrt{\bar{\alpha}_2}}\right)\sin\left(\omega_n\xi_{LS,1b}\right)-\sqrt{\bar{\alpha}_2}\sin\left(\frac{\gamma\omega_n}{\sqrt{\bar{\alpha}_2}}\right)\cos\left(\omega_n\xi_{LS,1b}\right)\right)-\sin\left(\frac{\omega_n\left(\xi_{LS,2a}-1\right)}{\sqrt{\bar{\alpha}_2}}\right)\left(\sqrt{\bar{\alpha}_2}\cos\left(\frac{\gamma\omega_n}{\sqrt{\bar{\alpha}_2}}\right)\cos\left(\omega_n\xi_{LS,1b}\right)\right.$$
$$\left.+\bar{k}_2\sin\left(\frac{\gamma\omega_n}{\sqrt{\bar{\alpha}_2}}\right)\sin\left(\omega_n\xi_{LS,1b}\right)\right)=0 \tag{14}$$

and the coefficients c_n are given by,

$$c_n=-\frac{1}{N_n}\left[\int_{\gamma-\xi_{LS,1b}}^{\gamma}\left(-\frac{\bar{k}_2\phi_2\left(\xi-\gamma+\xi_{LS,1b}\right)}{\gamma+\xi_{LS,2a}-\bar{k}_2\xi_{LS,1b}-1}\right)\left[\sin(\omega_n\xi)-\tan\left(\omega_n\left(\gamma-\xi_{LS,1b}\right)\right)\cos(\omega_n\xi)\right]d\xi\right.$$
$$+\frac{\bar{k}_2}{\bar{\alpha}_2}\int_{\gamma}^{1-\xi_{LS,2a}}\left(\phi_2-\frac{\phi_2\left(\xi+\xi_{LS,2a}-1\right)}{\gamma+\xi_{LS,2a}-\bar{k}_2\,\xi_{LS,1b}-1}\right)\left[\left(-\frac{\sqrt{\bar{\alpha}_2}\sin\left(\frac{\gamma\omega_n}{\sqrt{\bar{\alpha}_2}}\right)\cos\left(\omega_n\xi_{LS,1b}\right)}{\bar{k}_2\cos\left(\omega_n\left(\gamma-\xi_{LS,1b}\right)\right)}+\frac{\cos\left(\frac{\gamma\omega_n}{\sqrt{\bar{\alpha}_2}}\right)\sin\left(\omega_n\xi_{LS,1b}\right)}{\cos\left(\omega_n\left(\gamma-\xi_{LS,1b}\right)\right)}\right)\cos\left(\frac{\omega_n}{\sqrt{\bar{\alpha}_2}}\,\xi\right)\right. \tag{15}$$
$$\left.\left.+\left(\frac{\sqrt{\bar{\alpha}_2}\cos\left(\frac{\gamma\omega_n}{\sqrt{\bar{\alpha}_2}}\right)\cos\left(\omega_n\xi_{LS,1b}\right)}{\bar{k}_2\cos\left(\omega_n\left(\gamma-\xi_{LS,1b}\right)\right)}+\frac{\sin\left(\frac{\gamma\omega_n}{\sqrt{\bar{\alpha}_2}}\right)\sin\left(\omega_n\xi_{LS,1b}\right)}{\cos\left(\omega_n\left(\gamma-\xi_{LS,1b}\right)\right)}\right)\sin\left(\frac{\omega_n}{\sqrt{\bar{\alpha}_2}}\,\xi\right)\right]d\xi\right]$$

in which, the norms N_n are given by

$$N_n=\int_{\gamma-\xi_{LS,1b}}^{\gamma}\left[-\tan\left(\omega_n\left(\gamma-\xi_{LS,1b}\right)\right)\cos(\omega_n\xi)+\sin(\omega_n\xi)\right]^2d\xi+\frac{\bar{k}_2}{\bar{\alpha}_2}\int_{\gamma}^{1-\xi_{LS,2a}}\left[\left(-\frac{\sqrt{\bar{\alpha}_2}\sin\left(\frac{\gamma\omega_n}{\sqrt{\bar{\alpha}_2}}\right)\cos\left(\omega_n\xi_{LS,1b}\right)+\bar{k}_2\cos\left(\frac{\gamma\omega_n}{\sqrt{\bar{\alpha}_2}}\right)\sin\left(\omega_n\xi_{LS,1b}\right)}{\bar{k}_2\cos\left(\omega_n\left(\gamma-\xi_{LS,1b}\right)\right)}\right)\cos\left(\frac{\omega_n}{\sqrt{\bar{\alpha}_2}}\,\xi\right)\right.$$
$$\left.+\left(\frac{\sqrt{\bar{\alpha}_2}\cos\left(\frac{\gamma\omega_n}{\sqrt{\bar{\alpha}_2}}\right)\cos\left(\omega_n\xi_{LS,1b}\right)+\bar{k}_2\sin\left(\frac{\gamma\omega_n}{\sqrt{\bar{\alpha}_2}}\right)\sin\left(\omega_n\xi_{LS,1b}\right)}{\bar{k}_2\cos\left(\omega_n\left(\gamma-\xi_{LS,1b}\right)\right)}\right)\sin\left(\frac{\omega_n}{\sqrt{\bar{\alpha}_2}}\,\xi\right)\right]^2d\xi \tag{16}$$

The governing equation for layer 2a in the region $1-\xi_{LS,2a}<\xi<1$, which is uncoupled from the other layers may be written as,

$$\frac{\partial^2\theta_{2a}}{\partial\xi^2}=\frac{1}{\bar{\alpha}_2}\frac{\partial\theta_{2a}}{\partial\tau}\quad\left(1-\xi_{LS,2a}<\xi<1\right) \tag{17}$$

and the boundary conditions for this layer are given by

$$\theta_{2a} = \phi_2 \ (\xi = 1 - \xi_{LS,2a}) \tag{18}$$

$$\theta_{2a} = \theta_{w,2} \ (\xi = 1) \tag{19}$$

The method of separation of variables may be utilized to solve this problem, leading to the following solution for the temperature distribution in layer 2a,

$$\theta_{2a}(\xi,\tau) = \theta_{w,2} + \frac{(\theta_{w,2}-\phi_2)(\xi-1)}{\xi_{LS,2a}} + \sum_{n=1}^{\infty} \widetilde{c}_n \left[\cos\left(\frac{\widetilde{\omega}_n}{\sqrt{\bar{\alpha}_2}}\,\xi\right) + \cot\left(\frac{\widetilde{\omega}_n\left(\xi_{LS,2a}-1\right)}{\sqrt{\bar{\alpha}_2}}\right)\sin\left(\frac{\widetilde{\omega}_n}{\sqrt{\bar{\alpha}_2}}\,\xi\right)\right]\exp\left(-\widetilde{\omega}_n^2\tau\right) \tag{20}$$

where, the eigenvalues are $\widetilde{\omega}_n = \frac{\sqrt{\bar{\alpha}_2}}{\xi_{LS,2a}} n\pi \ (n = 1, 2, \ldots\infty)$ and the coefficients $\widetilde{c}_n$ are given by

$$\widetilde{c}_n = -\frac{1}{\widetilde{N}_n} \int_{1-\xi_{LS,2a}}^{1} \left(\theta_{w,2} + \frac{(\theta_{w,2}-\phi_2)(\xi-1)}{\xi_{LS,2a}}\right)\left(\cos\left(\frac{\widetilde{\omega}_n}{\sqrt{\bar{\alpha}_2}}\,\xi\right) + \cot\left(\frac{\widetilde{\omega}_n\left(\xi_{LS,2a}-1\right)}{\sqrt{\bar{\alpha}_2}}\right)\sin\left(\frac{\widetilde{\omega}_n}{\sqrt{\bar{\alpha}_2}}\,\xi\right)\right) d\xi \tag{21}$$

and the norms $\widetilde{N}_n$ are

$$\widetilde{N}_n = \int_{1-\xi_{LS,2a}}^{1} \left[\cos\left(\frac{\widetilde{\omega}_n}{\sqrt{\bar{\alpha}_2}}\,\xi\right) + \cot\left(\frac{\widetilde{\omega}_n\left(\xi_{LS,2a}-1\right)}{\sqrt{\bar{\alpha}_2}}\right)\sin\left(\frac{\widetilde{\omega}_n}{\sqrt{\bar{\alpha}_2}}\,\xi\right)\right]^2 d\xi \tag{22}$$

Once the temperature distributions in the four layers involved in Stage A are determined using Eqs. (4), (12), (13) and (20) above, the rates of propagation of the three melting fronts may be determined on the basis of energy conservation at each melting front. While $\xi_{LS,1a}$ is given explicitly by Eq. (5), the rates of propagation of $\xi_{LS,1b}$ and $\xi_{LS,2a}$ may be obtained on the basis of energy conservation at the respective melting fronts. Since all of the thermal energy needed to propagate the melting front over an infinitesimal time is supplied by net thermal conduction into the interface, therefore, the following expressions may be derived,

Stage A finishes at $\tau = \tau_A^*$ when all of layer 2 has finished melting i.e., $\xi_{LS,2a}(\tau_A^*) = 1 - \gamma$. The subsequent completion of melting of layer 1 occurs in Stage B, as described in the next sub-section. The final temperature field at $\tau = \tau_A^*$, which serves as an initial condition for Stage B, is given by,

$$\theta_{1a,A}^*(\xi) = 1 - \frac{\operatorname{erf}\left(\frac{\xi}{2\sqrt{\tau_A^*}}\right)}{\operatorname{erf}(\lambda)} \tag{25}$$

$$\frac{d\xi_{LS,1b}}{d\tau} = Ste_1\left(\frac{\partial\theta_{1b}}{\partial\xi}\right)_{\xi=\gamma-\xi_{LS,1b}} = Ste_1\left\{-\frac{\bar{k}_2\phi_2}{\gamma+\xi_{LS,2a}-\bar{k}_2\xi_{LS,1b}-1} + \sum_{n=1}^{\infty} c_n\omega_n\left[\tan\left(\omega_n\left(\gamma-\xi_{LS,1b}\right)\right)\sin\left(\omega_n\left(\gamma-\xi_{LS,1b}\right)\right) + \cos\left(\omega_n\left(\gamma-\xi_{LS,1b}\right)\right)\right]\exp\left(-\omega_n^2\tau\right)\right\} \tag{23}$$

$$\begin{aligned}\frac{d\xi_{LS,2a}}{d\tau} = Ste_2\bar{\alpha}_2\left(\frac{\partial\theta_{2a}}{\partial\xi} - \frac{\partial\theta_{2b}}{\partial\xi}\right)_{\xi=1-\xi_{LS,2a}} = Ste_2\bar{\alpha}_2\Bigg\{&\frac{\theta_{w,2}-\phi_2}{\xi_{LS,2a}} + \sum_{n=1}^{\infty}\frac{\widetilde{c}_n\widetilde{\omega}_n}{\sqrt{\bar{\alpha}_2}}\left[\cot\left(\frac{\widetilde{\omega}_n\left(\xi_{LS,2a}-1\right)}{\sqrt{\bar{\alpha}_2}}\right)\cos\left(\frac{\widetilde{\omega}_n\left(1-\xi_{LS,2a}\right)}{\sqrt{\bar{\alpha}_2}}\right) - \sin\left(\frac{\widetilde{\omega}_n\left(1-\xi_{LS,2a}\right)}{\sqrt{\bar{\alpha}_2}}\right)\right.\\ &\left.+\right]\exp\left(-\widetilde{\omega}_n^2\tau\right) + \frac{\phi_2}{\gamma+\xi_{LS,2a}-\bar{k}_2\xi_{LS,1b}-1} - \sum_{n=1}^{\infty}\frac{c_n\omega_n}{\sqrt{\bar{\alpha}_2}}\left[\left(\frac{\sqrt{\bar{\alpha}_2}\sin\left(\frac{\gamma\omega_n}{\sqrt{\bar{\alpha}_2}}\right)\cos\left(\omega_n\xi_{LS,1b}\right) - \bar{k}_2\cos\left(\frac{\gamma\,\omega_n}{\sqrt{\bar{\alpha}_2}}\right)\sin\left(\omega_n\xi_{LS,1b}\right)}{\bar{k}_2\cos\left(\omega_n\left(\gamma-\xi_{LS,1b}\right)\right)}\right)\sin\left(\frac{\omega_n\left(1-\xi_{LS,2a}\right)}{\sqrt{\bar{\alpha}_2}}\right)\right.\\ &\left.+\left(\frac{\sqrt{\bar{\alpha}_2}\cos\left(\frac{\gamma\omega_n}{\sqrt{\bar{\alpha}_2}}\right)\cos\left(\omega_n\xi_{LS,1b}\right) + \bar{k}_2\sin\left(\frac{\gamma\omega_n}{\sqrt{\bar{\alpha}_2}}\right)\sin\left(\omega_n\xi_{LS,1b}\right)}{\bar{k}_2\cos\left(\omega_n\left(\gamma-\xi_{LS,1b}\right)\right)}\right)\cos\left(\frac{\omega_n\left(1-\xi_{LS,2a}\right)}{\sqrt{\bar{\alpha}_2}}\right)\right]\exp\left(-\omega_n^2\tau\right)\Bigg\}\end{aligned} \tag{24}$$

$$\theta^*_{1b,A}(\xi)=\frac{\bar{k}_2\phi_2\left(\xi-\gamma+\xi^*_{LS,1b,A}\right)}{\bar{k}_2\xi^*_{LS,1b,A}}+\sum_{n=1}^{\infty}c_n\Big[-\tan\left(\omega_n\left(\gamma-\xi^*_{LS,1b,A}\right)\right)\cos(\omega_n\xi)+\sin(\omega_n\xi)\Big]\exp\left(-\omega_n^2\tau^*_A\right) \tag{26}$$

$$\begin{aligned}\theta^*_{2b,A}(\xi)=\phi_2+\frac{\phi_2(\xi-\gamma)}{\bar{k}_2\xi^*_{LS,1b,A}}+\sum_{n=1}^{\infty}c_n\Bigg[&\left(-\frac{\sqrt{\bar{\alpha}_2}\sin\left(\frac{\gamma\omega_n}{\sqrt{\bar{\alpha}_2}}\right)\cos\left(\omega_n\xi^*_{LS,1b,A}\right)-\bar{k}_2\cos\left(\frac{\gamma\omega_n}{\sqrt{\bar{\alpha}_2}}\right)\sin\left(\omega_n\xi^*_{LS,1b,A}\right)}{\bar{k}_2\cos\left(\omega_n\left(\gamma-\xi^*_{LS,1b,A}\right)\right)}\right)\cos\left(\frac{\omega_n}{\sqrt{\bar{\alpha}_2}}\xi\right)\\&+\left(\frac{\sqrt{\bar{\alpha}_2}\cos\left(\frac{\gamma\omega_n}{\sqrt{\bar{\alpha}_2}}\right)\cos\left(\omega_n\xi^*_{LS,1b,A}\right)+\bar{k}_2\sin\left(\frac{\gamma\omega_n}{\sqrt{\bar{\alpha}_2}}\right)\sin\left(\omega_n\xi^*_{LS,1b,A}\right)}{\bar{k}_2\cos\left(\omega_n\left(\gamma-\xi^*_{LS,1b,A}\right)\right)}\right)\sin\left(\frac{\omega_n}{\sqrt{\bar{\alpha}_2}}\xi\right)\Bigg]\exp\left(-\omega_n^2\tau^*_A\right)\end{aligned} \tag{27}$$

$$\theta^*_{2a,A}(\xi)=\theta_{w,2}+\frac{(\theta_{w,2}-\phi_2)(\xi-1)}{1-\gamma}+\sum_{n=1}^{\infty}\widetilde{c}_n\left[\cos\left(\frac{\widetilde{\omega}_n}{\sqrt{\bar{\alpha}_2}}\xi\right)-\cot\left(\frac{\widetilde{\omega}_n\gamma}{\sqrt{\bar{\alpha}_2}}\right)\sin\left(\frac{\widetilde{\omega}_n}{\sqrt{\bar{\alpha}_2}}\xi\right)\right]\exp\left(-\widetilde{\omega}_n^2\tau^*_A\right) \tag{28}$$

where $\xi^*_{LS,1b,A}$ is the location of the secondary melting front in layer 1 at the end of Stage A, which may be obtained by integrating Eq. (23) up to $\tau=\tau^*_A$.

2.1.2. Stage B: Completion of melting of layer 1

Since layer 2 finishes melting by the end of Stage A, therefore, only sensible heating occurs within this layer during the subsequent Stage B. In contrast, layer 1 continues to melt from both sides, resulting in the formation of four distinct layers, as shown in Fig. 2: 1a, 1b, 2 and an unmelted layer between layers 1a and 1b which remains at its melting temperature without any heat transfer.

Layer 1a continues to be characterized by the well-known Stefan problem with a constant wall temperature, for which, the governing equations, solution for the temperature distribution and melting front location as a function of time continue to be given by Eqs. (1)–(5).

Layers 1b and 2 are coupled at their interface, $\xi=\gamma$. The governing equations for layers 1b and 2 are given by

$$\frac{\partial^2\theta_{1b}}{\partial\xi^2}=\frac{\partial\theta_{1b}}{\partial\tau}\ \left(\gamma-\xi_{LS,1b}<\xi<\gamma\right) \tag{29}$$

$$\frac{\partial^2\theta_2}{\partial\xi^2}=\frac{1}{\bar{\alpha}_2}\frac{\partial\theta_2}{\partial\tau}\ (\gamma<\xi<1) \tag{30}$$

with the following interface and boundary conditions,

$$\theta_{1b}=0\ \left(\xi=\gamma-\xi_{LS,1b}\right) \tag{31}$$

$$\theta_{1b}=\theta_2\ (\xi=\gamma) \tag{32}$$

$$\frac{\partial\theta_{1b}}{\partial\xi}=\bar{k}_2\frac{\partial\theta_2}{\partial\xi}\ (\xi=\gamma) \tag{33}$$

$$\theta_2=\theta_{w,2}\ (\xi=1) \tag{34}$$

The initial condition for Stage B comes from the temperature distribution at the end of Stage A, $\tau=\tau^*_A$, using equations derived in the previous sub-section.

Following the same technique as described in the previous subsection, temperature distribution in the two layers may be derived as follows,

$$\begin{aligned}\theta_{1b}(\xi,\tau)=\frac{\bar{k}_2\theta_{w,2}\left(\xi-\gamma+\xi_{LS,1b}\right)}{\bar{k}_2\xi_{LS,1b}-\gamma+1}+\sum_{n=1}^{\infty}\widehat{c}_n\Big[&-\tan\left(\widehat{\omega}_n\left(\gamma-\xi_{LS,1b}\right)\right)\cos(\widehat{\omega}_n\xi)\\&+\sin(\widehat{\omega}_n\xi)\Big]\exp\left(-\widehat{\omega}_n^2\left(\tau-\tau^*_A\right)\right)\end{aligned} \tag{35}$$

$$\begin{aligned}\theta_2(\xi,\tau)=\theta_{w,2}+\frac{\theta_{w,2}(\xi-1)}{\bar{k}_2\xi_{LS,1b}-\gamma+1}+\sum_{n=1}^{\infty}\widehat{c}_n\Bigg[&\left(-\frac{\sqrt{\bar{\alpha}_2}\sin\left(\frac{\gamma\widehat{\omega}_n}{\sqrt{\bar{\alpha}_2}}\right)\cos\left(\widehat{\omega}_n\xi_{LS,1b}\right)}{\bar{k}_2\cos\left(\widehat{\omega}_n\left(\gamma-\xi_{LS,1b}\right)\right)}+\frac{\cos\left(\frac{\gamma\widehat{\omega}_n}{\sqrt{\bar{\alpha}_2}}\right)\sin\left(\widehat{\omega}_n\xi_{LS,1b}\right)}{\cos\left(\widehat{\omega}_n\left(\gamma-\xi_{LS,1b}\right)\right)}\right)\cos\left(\frac{\widehat{\omega}_n}{\sqrt{\bar{\alpha}_2}}\xi\right)\\&+\left(\frac{\sqrt{\bar{\alpha}_2}\cos\left(\frac{\gamma\widehat{\omega}_n}{\sqrt{\bar{\alpha}_2}}\right)\cos\left(\widehat{\omega}_n\xi_{LS,1b}\right)}{\bar{k}_2\cos\left(\widehat{\omega}_n\left(\gamma-\xi_{LS,1b}\right)\right)}+\frac{\sin\left(\frac{\gamma\widehat{\omega}_n}{\sqrt{\bar{\alpha}_2}}\right)\sin\left(\widehat{\omega}_n\xi_{LS,1b}\right)}{\cos\left(\widehat{\omega}_n\left(\gamma-\xi_{LS,1b}\right)\right)}\right)\sin\left(\frac{\widehat{\omega}_n}{\sqrt{\bar{\alpha}_2}}\xi\right)\Bigg]\exp\left(-\widehat{\omega}_n^2\left(\tau-\tau^*_A\right)\right)\end{aligned} \tag{36}$$

where the eigenvalues $\widehat{\omega}_n$ are roots of the following eigenfunction,

$$\sqrt{\bar{\alpha}_2}\sin\left(\frac{\widehat{\omega}_n}{\sqrt{\bar{\alpha}_2}}\right)\cos\left(\frac{\gamma\widehat{\omega}_n}{\sqrt{\bar{\alpha}_2}}\right)\cos\left(\widehat{\omega}_n\xi_{LS,1b}\right)-\sqrt{\bar{\alpha}_2}\sin\left(\frac{\gamma\widehat{\omega}_n}{\sqrt{\bar{\alpha}_2}}\right)\cos\left(\widehat{\omega}_n\xi_{LS,1b}\right)\cos\left(\frac{\widehat{\omega}_n}{\sqrt{\bar{\alpha}_2}}\right)+\bar{k}_2\cos\left(\frac{\gamma\widehat{\omega}_n}{\sqrt{\bar{\alpha}_2}}\right)\sin\left(\widehat{\omega}_n\xi_{LS,1b}\right)\cos\left(\frac{\widehat{\omega}_n}{\sqrt{\bar{\alpha}_2}}\right)$$
$$+\bar{k}_2\sin\left(\frac{\widehat{\omega}_n}{\sqrt{\bar{\alpha}_2}}\right)\sin\left(\frac{\gamma\widehat{\omega}_n}{\sqrt{\bar{\alpha}_2}}\right)\sin\left(\widehat{\omega}_n\xi_{LS,1b}\right)=0 \tag{37}$$

and the coefficients $\widehat{c}_n$ are given by

$$\widehat{c}_n=\frac{1}{\widehat{N}_n}\left[\int_{\gamma-\xi_{LS,1b}}^{\gamma}\left(\theta^*_{1b,A}(\xi)-\frac{\bar{k}_2\theta_{w,2}\left(\xi-\gamma+\xi_{LS,1b}\right)}{\bar{k}_2\xi_{LS,1b}-\gamma+1}\right)\left(-\tan\left(\widehat{\omega}_n\left(\gamma-\xi_{LS,1b}\right)\right)\cos\left(\widehat{\omega}_n\xi\right)+\sin\left(\widehat{\omega}_n\xi\right)\right)d\xi\right.$$
$$+\frac{\bar{k}_2}{\bar{\alpha}_2}\int_{\gamma}^{1}\left(\theta^*_{2a,A}(\xi)-\theta_{w,2}-\frac{\theta_{w,2}(\xi-1)}{\bar{k}_2\xi_{LS,1b}-\gamma+1}\right)\left(\left(-\frac{\sqrt{\bar{\alpha}_2}\sin\left(\frac{\gamma\widehat{\omega}_n}{\sqrt{\bar{\alpha}_2}}\right)\cos\left(\widehat{\omega}_n\xi_{LS,1b}\right)}{\bar{k}_2\cos\left(\widehat{\omega}_n\left(\gamma-\xi_{LS,1b}\right)\right)}+\frac{\cos\left(\frac{\gamma\widehat{\omega}_n}{\sqrt{\bar{\alpha}_2}}\right)\sin\left(\widehat{\omega}_n\xi_{LS,1b}\right)}{\cos\left(\widehat{\omega}_n\left(\gamma-\xi_{LS,1b}\right)\right)}\right)\cos\left(\frac{\widehat{\omega}_n}{\sqrt{\bar{\alpha}_2}}\xi\right)\right.$$
$$\left.\left.+\left(\frac{\sqrt{\bar{\alpha}_2}\cos\left(\frac{\gamma\widehat{\omega}_n}{\sqrt{\bar{\alpha}_2}}\right)\cos\left(\widehat{\omega}_n\xi_{LS,1b}\right)}{\bar{k}_2\cos\left(\widehat{\omega}_n\left(\gamma-\xi_{LS,1b}\right)\right)}+\frac{\sin\left(\frac{\gamma\widehat{\omega}_n}{\sqrt{\bar{\alpha}_2}}\right)\sin\left(\widehat{\omega}_n\xi_{LS,1b}\right)}{\cos\left(\widehat{\omega}_n\left(\gamma-\xi_{LS,1b}\right)\right)}\right)\sin\left(\frac{\widehat{\omega}_n}{\sqrt{\bar{\alpha}_2}}\xi\right)\right)d\xi\right] \tag{38}$$

where $\theta^*_{1b,A}$ and $\theta^*_{2a,A}$ are the initial temperature fields at the start of Stage B, given by Eqs. (26) and (28), respectively. In addition, the norm $\widehat{N}_n$ is given by

$$\widehat{N}_n=\int_{\gamma-\xi_{LS,1b}}^{\gamma}\left[-\tan\left(\widehat{\omega}_n\left(\gamma-\xi_{LS,1b}\right)\right)\cos\left(\widehat{\omega}_n\xi\right)+\sin\left(\widehat{\omega}_n\xi\right)\right]^2d\xi+\frac{\bar{k}_2}{\bar{\alpha}_2}\int_{\gamma}^{1}\left[\left(-\frac{\sqrt{\bar{\alpha}_2}\sin\left(\frac{\gamma\widehat{\omega}_n}{\sqrt{\bar{\alpha}_2}}\right)\cos\left(\widehat{\omega}_n\xi_{LS,1b}\right)}{\bar{k}_2\cos\left(\widehat{\omega}_n\left(\gamma-\xi_{LS,1b}\right)\right)}+\frac{\cos\left(\frac{\gamma\widehat{\omega}_n}{\sqrt{\bar{\alpha}_2}}\right)\sin\left(\widehat{\omega}_n\xi_{LS,1b}\right)}{\cos\left(\widehat{\omega}_n\left(\gamma-\xi_{LS,1b}\right)\right)}\right)\cos\left(\frac{\widehat{\omega}_n}{\sqrt{\bar{\alpha}_2}}\xi\right)\right.$$
$$\left.+\left(\frac{\sqrt{\bar{\alpha}_2}\cos\left(\frac{\gamma\widehat{\omega}_n}{\sqrt{\bar{\alpha}_2}}\right)\cos\left(\widehat{\omega}_n\xi_{LS,1b}\right)}{\bar{k}_2\cos\left(\widehat{\omega}_n\left(\gamma-\xi_{LS,1b}\right)\right)}+\frac{\sin\left(\frac{\gamma\widehat{\omega}_n}{\sqrt{\bar{\alpha}_2}}\right)\sin\left(\widehat{\omega}_n\xi_{LS,1b}\right)}{\cos\left(\widehat{\omega}_n\left(\gamma-\xi_{LS,1b}\right)\right)}\right)\sin\left(\frac{\widehat{\omega}_n}{\sqrt{\bar{\alpha}_2}}\xi\right)\right]^2d\xi \tag{39}$$

Once the temperature distribution is determined from Eq. (35), the rate of propagation of the melting front location for layer 1b is obtained using energy conservation at the interface, similar to the previous subsection, as,

$$\frac{d\xi_{LS,1b}}{d\tau}=Ste_1\left(\frac{\partial\theta_{1b}}{\partial\xi}\right)_{\xi=\gamma-\xi_{LS,1b}}=Ste_1\left\{\frac{\bar{k}_2\theta_{w,2}}{\bar{k}_2\xi_{LS,1b}-\gamma+1}+\sum_{n=1}^{\infty}\widehat{c}_n\widehat{\omega}_n\left[\tan\left(\widehat{\omega}_n\left(\gamma-\xi_{LS,1b}\right)\right)\sin\left(\widehat{\omega}_n\left(\gamma-\xi_{LS,1b}\right)\right)+\cos\left(\widehat{\omega}_n\left(\gamma-\xi_{LS,1b}\right)\right)\right]\exp\left(-\widehat{\omega}_n^2\left(\tau-\tau^*_A\right)\right)\right\} \tag{40}$$

Stage B, and consequently, the entire melting process ends at $\tau=\tau^*_B$, when layer 1 is entirely melted. This occurs when the two melting fronts in layer 1 have propagated inwards sufficiently, so as to meet and completely consume the unmelted region between the two. Mathemat-

ically, this is given simply by, $\xi_{LS,1a}(\tau_B^*) + \xi_{LS,1b}(\tau_B^*) = \gamma$.

2.2. Case II: Layer 1 finishes melting first

The Case described in the previous section is one in which layer 2 finishes melting first during Stage A of the phase change process. In contrast, under certain conditions, such as very thin layer 1, very high left wall temperature and/or very low latent heat of phase change of layer 1 material, it is possible that layer 1 finishes melting first instead during Stage A. This scenario, referred to as Case II, is considered in detail in this section.

The mathematical modeling of Stage A for this case is essentially identical to the previous case described in Section 2.1. Subsequently, in Stage B, layer 2 continues to melt, while there is sensible heating in layer 1 and the melted region of layer 2. As shown in Fig. 2, Stage B may end with completion of the entire melting process, or, under specific conditions, it is possible that the temperature at the interface between layers may rise enough to reach the melting temperature of layer 2 before complete melting of layer 2. If so, this will result in a secondary melting front in layer 2 that propagates rightwards, driven by heat transfer through the melted layer 1. This stage, referred to as Stage C is conditional upon sufficient heating of the inter-layer interface and only occurs in Case II.

The non-dimensionalization followed for Case II is the same as the one introduced in Section 2.1. Based on such non-dimensionalization, the conservation equations that govern the temperature field and melting propagation are described for each Stage below. Similar to Case I, these equations are also solved using the method of eigenfunction expansion. The following sub-sections describe the three Stages that may occur during melting of the two-PCM composite when Case II applies.

2.2.1. Stage A: Simultaneous melting of both layers

During Stage A, melting occurs in both layers 1 and 2. The thermal conduction and phase change process during Stage A is identical to Stage A of Case I, described in Section 2.1.1 above. The only difference is that unlike Case I, Stage A in Case II finishes when layer 1 finishes melting first, i.e., at $\tau = \tau_A^*$, at which, $\xi_{LS,1a}(\tau_A^*) + \xi_{LS,1b}(\tau_A^*) = \gamma$, where $\xi_{LS,1a}$ is given by Eq. (5) and $\xi_{LS,1b}$ is obtained by integrating Eq. (23).

2.2.2. Stage B: Further left-wards melting of layer 2

During Stage B, layer 1 experiences sensible heating, while layer 2 undergoes sensible heating in the already melted region and further melting of the region that remained unmelted at the end of Stage A. Three distinct layers exist during this Stage – layer 1, which is completely melted, layers 2a and 2b that refer to the melted and unmelted parts of layer 2, respectively. While the equations for layers 1 and 2b are coupled to each other through the interface at $\xi = \gamma$, equations for layer 2a are independent of the other layers. The temperature fields in layers 1 and 2b are governed by,

$$\frac{\partial^2\theta_1}{\partial\xi^2} = \frac{\partial\theta_1}{\partial\tau} \ (0 < \xi < \gamma) \tag{41}$$

$$\frac{\partial^2\theta_{2b}}{\partial\xi^2} = \frac{1}{\bar{\alpha}_2}\frac{\partial\theta_{2b}}{\partial\tau} \ \left(\gamma < \xi < 1 - \xi_{LS,2a}\right) \tag{42}$$

along with the following boundary conditions,

$$\theta_1 = 1 \ (\xi = 0) \tag{43}$$

$$\theta_1 = \theta_{2b} \ (\xi = \gamma) \tag{44}$$

$$\frac{\partial\theta_1}{\partial\xi} = \bar{k}_2\frac{\partial\theta_{2b}}{\partial\xi} \ (\xi = \gamma) \tag{45}$$

$$\theta_{2b} = \phi_2 \ \left(\xi = 1 - \xi_{LS,2a}\right) \tag{46}$$

The initial condition for Stage B comes from the temperature distribution at the end of Stage A, $\tau = \tau_A^*$, using equations derived in the previous sub-section.

Using the same technique as previous sub-sections, the temperature distribution may be obtained as,

$$\theta_1(\xi,\tau) = \frac{\bar{k}_2\xi(\phi_2 - 1)}{\gamma(\bar{k}_2 - 1) - \xi_{LS,2a} + 1} + 1 + \sum_{n=1}^{\infty} \mathring{c}_n \sin\left(\mathring{\omega}_n\xi\right)\exp\left(-\mathring{\omega}_n^2\left(\tau - \tau_A^*\right)\right) \tag{47}$$

$$\theta_{2b}(\xi,\tau) = \phi_2 + \frac{(\phi_2 - 1)\left(\xi + \xi_{LS,2a} - 1\right)}{\gamma(\bar{k}_2 - 1) - \xi_{LS,2a} + 1} + \sum_{n=1}^{\infty} \mathring{c}_n \left[\left(\cos\left(\frac{\gamma\mathring{\omega}_n}{\sqrt{\bar{\alpha}_2}}\right)\sin\left(\gamma\mathring{\omega}_n\right) - \frac{\sqrt{\bar{\alpha}_2}}{\bar{k}_2}\sin\left(\frac{\gamma\mathring{\omega}_n}{\sqrt{\bar{\alpha}_2}}\right)\cos\left(\gamma\mathring{\omega}_n\right)\right)\cos\left(\frac{\mathring{\omega}_n}{\sqrt{\bar{\alpha}_2}}\xi\right) + \left(\sin\left(\frac{\gamma\mathring{\omega}_n}{\sqrt{\bar{\alpha}_2}}\right)\sin\left(\gamma\mathring{\omega}_n\right) + \frac{\sqrt{\bar{\alpha}_2}}{\bar{k}_2}\cos\left(\frac{\gamma\mathring{\omega}_n}{\sqrt{\bar{\alpha}_2}}\right)\cos\left(\gamma\mathring{\omega}_n\right)\right)\sin\left(\frac{\mathring{\omega}_n}{\sqrt{\bar{\alpha}_2}}\xi\right)\right]\exp\left(-\mathring{\omega}_n^2\left(\tau - \tau_A^*\right)\right) \tag{48}$$

where the eigenequation associated with the eigenvalues $\mathring{\omega}_n$ is

$$\bar{k}_2\cos\left(\frac{\gamma\mathring{\omega}_n}{\sqrt{\bar{\alpha}_2}}\right)\sin\left(\gamma\mathring{\omega}_n\right)\cos\left(\frac{\mathring{\omega}_n\left(\xi_{LS,2a} - 1\right)}{\sqrt{\bar{\alpha}_2}}\right) - \bar{k}_2\sin\left(\frac{\gamma\mathring{\omega}_n}{\sqrt{\bar{\alpha}_2}}\right)\sin\left(\gamma\mathring{\omega}_n\right)\sin\left(\frac{\mathring{\omega}_n\left(\xi_{LS,2a} - 1\right)}{\sqrt{\bar{\alpha}_2}}\right) - \sqrt{\bar{\alpha}_2}\cos\left(\frac{\gamma\mathring{\omega}_n}{\sqrt{\bar{\alpha}_2}}\right)\cos\left(\gamma\mathring{\omega}_n\right)\sin\left(\frac{\mathring{\omega}_n\left(\xi_{LS,2a} - 1\right)}{\sqrt{\bar{\alpha}_2}}\right) - \sqrt{\bar{\alpha}_2}\sin\left(\frac{\gamma\mathring{\omega}_n}{\sqrt{\bar{\alpha}_2}}\right)\cos\left(\gamma\mathring{\omega}_n\right)\cos\left(\frac{\mathring{\omega}_n\left(\xi_{LS,2a} - 1\right)}{\sqrt{\bar{\alpha}_2}}\right) = 0 \tag{49}$$

and coefficients $\mathring{c}_n$ are given by

$$\breve{c}_n = \frac{1}{\breve{N}_n}\left[\int_0^{\xi_{LS,1a}}\left(\theta^*_{1a,A}(\xi) - \frac{\bar{k}_2\xi(\phi_2-1)}{\gamma(\bar{k}_2-1)-\xi_{LS,2a}+1} - 1\right)\sin\left(\breve{\omega}_n\xi\right)d\xi + \int_{\xi_{LS,1a}}^{\gamma}\left(\theta^*_{1b,A}(\xi) - \frac{\bar{k}_2\xi(\phi_2-1)}{\gamma(\bar{k}_2-1)-\xi_{LS,2a}+1} - 1\right)\sin\left(\breve{\omega}_n\xi\right)d\xi \right.$$
$$+\frac{\bar{k}_2}{\bar{\alpha}_2}\int_{\gamma}^{1-\xi_{LS,2a}}\left(\theta^*_{2b,A}(\xi) - \phi_2 - \frac{(\phi_2-1)(\xi+\xi_{LS,2a}-1)}{\gamma(\bar{k}_2-1)-\xi_{LS,2a}+1}\right)\left(\cos\left(\frac{\gamma\breve{\omega}_n}{\sqrt{\bar{\alpha}_2}}\right)\sin\left(\gamma\breve{\omega}_n\right) - \frac{\sqrt{\bar{\alpha}_2}}{\bar{k}_2}\sin\left(\frac{\gamma\breve{\omega}_n}{\sqrt{\bar{\alpha}_2}}\right)\cos\left(\gamma\breve{\omega}_n\right)\right)\cos\left(\frac{\breve{\omega}_n}{\sqrt{\bar{\alpha}_2}}\xi\right) + \left(\sin\left(\frac{\gamma\breve{\omega}_n}{\sqrt{\bar{\alpha}_2}}\right)\sin\left(\gamma\breve{\omega}_n\right)\right.$$
$$\left.\left. + \frac{\sqrt{\bar{\alpha}_2}}{\bar{k}_2}\cos\left(\frac{\gamma\breve{\omega}_n}{\sqrt{\bar{\alpha}_2}}\right)\cos\left(\gamma\breve{\omega}_n\right)\right)\sin\left(\frac{\breve{\omega}_n}{\sqrt{\bar{\alpha}_2}}\xi\right)d\xi\right] \tag{50}$$

and the norms $\breve{N}_n$ are given by,

$$\breve{N}_n = \int_0^{\gamma}\sin^2\left(\widetilde{\omega}_n\xi\right)d\xi + \frac{\bar{k}_2}{\bar{\alpha}_2}\int_{\gamma}^{1-\xi_{LS,2a}}\left(\left(\cos\left(\frac{\gamma\breve{\omega}_n}{\sqrt{\bar{\alpha}_2}}\right)\sin\left(\gamma\breve{\omega}_n\right) - \frac{\sqrt{\bar{\alpha}_2}}{\bar{k}_2}\sin\left(\frac{\gamma\breve{\omega}_n}{\sqrt{\bar{\alpha}_2}}\right)\cos\left(\gamma\breve{\omega}_n\right)\right)\cos\left(\frac{\breve{\omega}_n}{\sqrt{\bar{\alpha}_2}}\xi\right) + \left(\sin\left(\frac{\gamma\breve{\omega}_n}{\sqrt{\bar{\alpha}_2}}\right)\sin\left(\gamma\breve{\omega}_n\right)\right.\right.$$
$$\left.\left. + \frac{\sqrt{\bar{\alpha}_2}}{\bar{k}_2}\cos\left(\frac{\gamma\breve{\omega}_n}{\sqrt{\bar{\alpha}_2}}\right)\cos\left(\gamma\breve{\omega}_n\right)\right)\sin\left(\frac{\breve{\omega}_n}{\sqrt{\bar{\alpha}_2}}\xi\right)\right)^2 d\xi \tag{51}$$

Here, $\theta^*_{1a,A}$, $\theta^*_{1b,A}$ and $\theta^*_{2b,A}$ refer to temperature fields at the end of Stage A. Since Stage A is identical for both cases, these temperature fields continue to be given by Eqs. (25)–(27), with τ^*_A given by the root of $\xi_{LS,1a}(\tau^*_A) + \xi_{LS,1b}(\tau^*_A) = \gamma$.

The governing equations, boundary conditions and temperature distribution for layer 2a, which is uncoupled from the other layers continue to be given by Eqs. (17)–(22), and the rate of phase change front location in layer 2a by Eq. (24). The temperature distribution at the end of this stage i.e., $\tau = \tau^*_B$, may be written as,

$$\theta^*_{1,B}(\xi) = \frac{\bar{k}_2\xi(\phi_2-1)}{\gamma(\bar{k}_2-1)-\xi_{LS,2a}+1} + 1 + \sum_{n=1}^{\infty}\breve{c}_n\sin\left(\breve{\omega}_n\xi\right)\exp\left(-\breve{\omega}_n^2\left(\tau^*_B-\tau^*_A\right)\right) \tag{52}$$

where the time of completion of Stage B, τ^*_B depends on whether temperature at the interface reaches the melting temperature of layer 2 before layer 2 finishes melting, as discussed next.

An interesting aspect of Stage B is that if before complete melting of layer 2, i.e., $\xi_{LS,2a}(\tau) < 1-\gamma$, the temperature at the interface reaches the melting temperature of layer 2 i.e., $\theta^*_{2a,B}(\gamma,\tau) = \phi_2$, then, an additional secondary melting front in layer 2 starts at the interface and begins to propagate rightwards due to heat transfer from the left wall through layer 1. This time period is referred to as Stage C. Instead, if the interface temperature remains under ϕ_2, i.e., if $\theta^*_{2a,B}(\gamma,\tau) \le \phi_2$ when $\xi_{LS2a}(\tau) = 1-\gamma$, then the entire melting process will finish at the end of Stage B due to complete melting of layer 2 only from the right wall. Therefore, a conditional Stage C exists in this scenario, as shown in Fig. 2. The mathematical modeling of Stage C, if it occurs, is discussed in the next subsection.

2.2.3. Stage C: Melting of layer 2 in both directions

This Stage is characterized by four different layers - layer 1, which is already completely melted, layers 2a and layer 2b, which represent melted regions in layer 2 due to phase change fronts from the right and left, respectively, and layer 2c which is an unmelted layer between layers 2a and 2b. The governing equation, boundary conditions and temperature distribution for layer 2a remains the same as Stage A, given by Eqs. (17)–(22). The rate of change of phase change propagation for layer 2a can also be found using Eq. (24) by substituting τ with $(\tau-\tau^*_B)$. In addition, the governing equations for layers 1 and 2b are the same as Eqs. (41) and (42), along with the following boundary conditions,

$$\theta_1 = 1 \ (\xi = 0) \tag{54}$$

$$\theta^*_{2b,B}(\xi) = \phi_2 + \frac{(\phi_2-1)(\xi+\xi_{LS,2a}-1)}{\gamma(\bar{k}_2-1)-\xi_{LS,2a}+1} + \sum_{n=1}^{\infty}\breve{c}_n\left[\left(\cos\left(\frac{\gamma\breve{\omega}_n}{\sqrt{\bar{\alpha}_2}}\right)\sin\left(\gamma\breve{\omega}_n\right) - \frac{\sqrt{\bar{\alpha}_2}}{\bar{k}_2}\sin\left(\frac{\gamma\breve{\omega}_n}{\sqrt{\bar{\alpha}_2}}\right)\cos\left(\gamma\breve{\omega}_n\right)\right)\cos\left(\frac{\breve{\omega}_n}{\sqrt{\bar{\alpha}_2}}\xi\right) + \left(\sin\left(\frac{\gamma\breve{\omega}_n}{\sqrt{\bar{\alpha}_2}}\right)\sin\left(\gamma\breve{\omega}_n\right)\right.\right.$$
$$\left.\left. + \frac{\sqrt{\bar{\alpha}_2}}{\bar{k}_2}\cos\left(\frac{\gamma\breve{\omega}_n}{\sqrt{\bar{\alpha}_2}}\right)\cos\left(\gamma\breve{\omega}_n\right)\right)\sin\left(\frac{\breve{\omega}_n}{\sqrt{\bar{\alpha}_2}}\xi\right)\right]\exp\left(-\breve{\omega}_n^2\left(\tau^*_B-\tau^*_A\right)\right) \tag{53}$$

$$\theta_1 = \theta_{2b}\ (\xi = \gamma) \tag{55}$$

$$\frac{\partial \theta_1}{\partial \xi} = \bar{k}_2 \frac{\partial \theta_{2b}}{\partial \xi}\ (\xi = \gamma) \tag{56}$$

$$\theta_{2b} = \phi_2\ \left(\xi = \gamma + \xi_{LS,2b}\right) \tag{57}$$

The initial condition for Stage C comes from the temperature distribution at the end of Stage B, $\tau = \tau_B^*$, using equations derived in the previous sub-section.

Temperature fields in layers 1 and 2b may be derived as,

$$\theta_1(\xi,\tau) = \frac{\bar{k}_2 \xi(\phi_2 - 1)}{\xi_{LS,2b} + \gamma \bar{k}_2} + 1 + \sum_{n=1}^{\infty} \breve{c}_n \sin(\breve{\omega}_n \xi) \exp\left(-\breve{\omega}_n^2 \left(\tau - \tau_B^*\right)\right) \tag{58}$$

and the eigenvalues are given by roots of,

$$\sqrt{\bar{\alpha}_2} \sin\left(\frac{\breve{\omega}_n \xi_{LS,2b}}{\sqrt{\bar{\alpha}_2}}\right) \cos(\gamma \breve{\omega}_n) + \bar{k}_2 \cos\left(\frac{\breve{\omega}_n \xi_{LS,2b}}{\sqrt{\bar{\alpha}_2}}\right) \sin(\gamma \breve{\omega}_n) = 0 \tag{60}$$

Here, the coefficients $\breve{c}_n$ are given by

$$\breve{c}_n = \frac{1}{\breve{N}_n} \left[\int_0^{\gamma} \left(\theta_{1,B}^*(\xi) - \frac{\bar{k}_2 \xi(\phi_2 - 1)}{\xi_{LS,2b} + \gamma \bar{k}_2} + 1 \right) \sin(\breve{\omega}_n \xi) d\xi + \frac{\bar{k}_2}{\bar{\alpha}_2} \int_{\gamma}^{\gamma + \xi_{LS,2b}} \left(\theta_{2b,B}^*(\xi) - \phi_2 + \frac{(\phi_2 - 1)\left(\gamma - \xi + \xi_{LS,2b}\right)}{\xi_{LS,2b} + \gamma \bar{k}_2} \right) \left(\cos\left(\frac{\gamma \breve{\omega}_n}{\sqrt{\bar{\alpha}_2}}\right) \sin(\gamma \breve{\omega}_n) \right.$$
$$\left. - \frac{\sqrt{\bar{\alpha}_2}}{\bar{k}_2} \sin\left(\frac{\gamma \breve{\omega}_n}{\sqrt{\bar{\alpha}_2}}\right) \cos(\gamma \breve{\omega}_n) \right) \cos\left(\frac{\breve{\omega}_n}{\sqrt{\bar{\alpha}_2}} \xi\right) + \left(\sin\left(\frac{\gamma \breve{\omega}_n}{\sqrt{\bar{\alpha}_2}}\right) \sin(\gamma \breve{\omega}_n) + \frac{\sqrt{\bar{\alpha}_2}}{\bar{k}_2} \cos\left(\frac{\gamma \breve{\omega}_n}{\sqrt{\bar{\alpha}_2}}\right) \cos(\gamma \breve{\omega}_n) \right) \sin\left(\frac{\breve{\omega}_n}{\sqrt{\bar{\alpha}_2}} \xi\right) d\xi \Bigg] \tag{61}$$

in which, the norms $\breve{N}_n$ are given by,

$$\breve{N}_n = \int_0^{\gamma} \sin^2(\breve{\omega}_n \xi) d\xi + \frac{\bar{k}_2}{\bar{\alpha}_2} \int_{\gamma}^{\gamma + \xi_{LS,2b}} \left(\left(\cos\left(\frac{\gamma \breve{\omega}_n}{\sqrt{\bar{\alpha}_2}}\right) \sin(\gamma \breve{\omega}_n) - \frac{\sqrt{\bar{\alpha}_2}}{\bar{k}_2} \sin\left(\frac{\gamma \breve{\omega}_n}{\sqrt{\bar{\alpha}_2}}\right) \cos(\gamma \breve{\omega}_n) \right) \cos\left(\frac{\breve{\omega}_n}{\sqrt{\bar{\alpha}_2}} \xi\right) + \left(\sin\left(\frac{\gamma \breve{\omega}_n}{\sqrt{\bar{\alpha}_2}}\right) \sin(\gamma \breve{\omega}_n) + \frac{\sqrt{\bar{\alpha}_2}}{\bar{k}_2} \cos\left(\frac{\gamma \breve{\omega}_n}{\sqrt{\bar{\alpha}_2}}\right) \cos(\gamma \breve{\omega}_n) \right) \sin\left(\frac{\breve{\omega}_n}{\sqrt{\bar{\alpha}_2}} \xi\right) \right)^2 d\xi \tag{62}$$

Finally, the layer 2c problem is a pure conduction problem, with the following governing equation,

$$\frac{\partial^2 \theta_{2c}}{\partial \xi^2} = \frac{1}{\bar{\alpha}_2} \frac{\partial \theta_{2c}}{\partial \tau}\ \left(\gamma + \xi_{LS,2b} < \xi < 1 - \xi_{LS,2a}\right) \tag{63}$$

along with the following boundary conditions

$$\theta_{2c} = \phi_2\ \left(\xi = \gamma + \xi_{LS,2b}\right) \tag{64}$$

$$\theta_{2c} = \phi_2\ \left(\xi = 1 - \xi_{LS,2a}\right) \tag{65}$$

and a zero initial condition. Note that heat transfer into layer 2c occurs despite both ends at the same temperature because layer 2c is initially cooler than its melting temperature.

$$\theta_{2b}(\xi,\tau) = \phi_2 - \frac{(\phi_2 - 1)\left(\gamma - \xi + \xi_{LS,2b}\right)}{\xi_{LS,2b} + \gamma \bar{k}_2} + \sum_{n=1}^{\infty} \breve{c}_n \left[\left(\cos\left(\gamma \frac{\breve{\omega}_n}{\sqrt{\bar{\alpha}_2}}\right) \sin(\gamma \breve{\omega}_n) - \frac{\sqrt{\bar{\alpha}_2}}{\bar{k}_2} \sin\left(\gamma \frac{\breve{\omega}_n}{\sqrt{\bar{\alpha}_2}}\right) \cos(\gamma \breve{\omega}_n) \right) \cos\left(\frac{\breve{\omega}_n}{\sqrt{\bar{\alpha}_2}} \xi\right) + \left(\sin\left(\gamma \frac{\breve{\omega}_n}{\sqrt{\bar{\alpha}_2}}\right) \sin(\gamma \breve{\omega}_n) \right.$$
$$\left. + \frac{\sqrt{\bar{\alpha}_2}}{\bar{k}_2} \cos\left(\gamma \frac{\breve{\omega}_n}{\sqrt{\bar{\alpha}_2}}\right) \cos(\gamma \breve{\omega}_n) \right) \sin\left(\frac{\breve{\omega}_n}{\sqrt{\bar{\alpha}_2}} \xi\right) \Bigg] \exp\left(-\breve{\omega}_n^2 \left(\tau - \tau_B^*\right)\right) \tag{59}$$

The temperature distribution in layer 2c may be determined by solving the conduction problem as follows,

$$\theta_{2c}(\xi,\tau)=\phi_2+\sum_{n=1}^{\infty}\widehat{c}_n\left[\cos\left(\frac{\widehat{\omega}_n}{\sqrt{\bar{\alpha}_2}}\xi\right)-\cot\left(\frac{\widehat{\omega}_n(\gamma+\xi_{LS,2b})}{\sqrt{\bar{\alpha}_2}}\right)\sin\left(\frac{\widehat{\omega}_n}{\sqrt{\bar{\alpha}_2}}\xi\right)\right]\exp\left(-\widehat{\omega}_n^2(\tau-\tau_B^*)\right) \tag{66}$$

where the eigenvalues are given by $\widehat{\omega}_n=\frac{\sqrt{\bar{\alpha}_2}}{(\gamma+\xi_{LS,2a}+\xi_{LS,2b}-1)}n\pi$ ($n=1,2,..,\infty$), and the coefficients $\widehat{c}_n$ are as follows,

$$\widehat{c}_n=\frac{1}{\widehat{N}_n}\left[\int_{\gamma+\xi_{LS,2b}}^{1-\xi_{LS,2a}}\left(\theta_{2b,B}^*(\xi)-\phi_2\right)\left(\cos\left(\frac{\widehat{\omega}_n}{\sqrt{\bar{\alpha}_2}}\xi\right)-\cot\left(\frac{\widehat{\omega}_n(\gamma+\xi_{LS,2b})}{\sqrt{\bar{\alpha}_2}}\right)\sin\left(\frac{\widehat{\omega}_n}{\sqrt{\bar{\alpha}_2}}\xi\right)\right)d\xi\right] \tag{67}$$

and $\widehat{N}_n$ are given by,

$$\widehat{N}_n=\int_{\gamma+\xi_{LS,2b}}^{1-\xi_{LS,2a}}\left(\cos\left(\frac{\widehat{\omega}_n}{\sqrt{\bar{\alpha}_2}}\xi\right)-\cot\left(\frac{\widehat{\omega}_n(\gamma+\xi_{LS,2b})}{\sqrt{\bar{\alpha}_2}}\right)\sin\left(\frac{\widehat{\omega}_n}{\sqrt{\bar{\alpha}_2}}\xi\right)\right)^2d\xi \tag{68}$$

Finally, the rates of propagation of phase change locations are given by,

$$\begin{aligned}\frac{d\xi_{LS,2a}}{d\tau}&=Ste_2\bar{\alpha}_2\left(\frac{\partial\theta_{2a}}{\partial\xi}-\frac{\partial\theta_{2c}}{\partial\xi}\right)_{\xi=1-\xi_{LS,2a}}\\&=Ste_2\bar{\alpha}_2\left\{\left[\frac{\theta_{w,2}-\phi_2}{\xi_{LS,2a}}+\sum_{n=1}^{\infty}\frac{\widetilde{c}_n\widetilde{\omega}_n}{\sqrt{\bar{\alpha}_2}}\left[\cot\left(\frac{\widetilde{\omega}_n(\xi_{LS,2a}-1)}{\sqrt{\bar{\alpha}_2}}\right)\cos\left(\frac{\widetilde{\omega}_n(1-\xi_{LS,2a})}{\sqrt{\bar{\alpha}_2}}\right)-\sin\left(\frac{\widetilde{\omega}_n(1-\xi_{LS,2a})}{\sqrt{\bar{\alpha}_2}}\right)\right]\exp\left(-\widetilde{\omega}_n^2(\tau-\tau_B^*)\right)\right)\right]\\&+\sum_{n=1}^{\infty}\bar{c}_n\frac{\widehat{\omega}_n}{\sqrt{\bar{\alpha}_2}}\left[\sin\left(\frac{\widehat{\omega}_n(1-\xi_{LS,2a})}{\sqrt{\bar{\alpha}_2}}\right)+\cot\left(\frac{\widehat{\omega}_n(\gamma+\xi_{LS,2b})}{\sqrt{\bar{\alpha}_2}}\right)\cos\left(\frac{\widehat{\omega}_n(1-\xi_{LS,2a})}{\sqrt{\bar{\alpha}_2}}\right)\right]\exp\left(-\widehat{\omega}_n^2(\tau-\tau_B^*)\right)\Bigg\}\end{aligned} \tag{69}$$

$$\begin{aligned}\frac{d\xi_{LS,2b}}{d\tau}&=Ste_2\bar{\alpha}_2\left(\frac{\partial\theta_{2c}}{\partial\xi}-\frac{\partial\theta_{2b}}{\partial\xi}\right)_{\xi=\gamma+\xi_{LS,2b}}\\&=-Ste_2\bar{\alpha}_2\Bigg\{\sum_{n=1}^{\infty}\frac{\widehat{c}_n\widehat{\omega}_n}{\sqrt{\bar{\alpha}_2}}\left[\sin\left(\frac{\widehat{\omega}_n(\gamma+\xi_{LS,2b})}{\sqrt{\bar{\alpha}_2}}\right)+\cot\left(\frac{\widehat{\omega}_n(\gamma+\xi_{LS,2b})}{\sqrt{\bar{\alpha}_2}}\right)\cos\left(\frac{\widehat{\omega}_n(\gamma+\xi_{LS,2b})}{\sqrt{\bar{\alpha}_2}}\right)\right]\exp\left(-\widehat{\omega}_n^2(\tau-\tau_B^*)\right)+\left[\frac{\phi_2-1}{\xi_{LS,2b}}\right.\\&\left.+\gamma\bar{k}_2+\sum_{n=1}^{\infty}\breve{c}_n\frac{\breve{\omega}_n}{\sqrt{\bar{\alpha}_2}}\left[\left(\frac{\sqrt{\bar{\alpha}_2}}{\bar{k}_2}\sin\left(\gamma\frac{\breve{\omega}_n}{\sqrt{\bar{\alpha}_2}}\right)\cos(\gamma\breve{\omega}_n)-\cos\left(\gamma\frac{\breve{\omega}_n}{\sqrt{\bar{\alpha}_2}}\right)\sin(\gamma\breve{\omega}_n)\right)\sin\left(\frac{\breve{\omega}_n(\gamma+\xi_{LS,2b})}{\sqrt{\bar{\alpha}_2}}\right)+\left(\sin\left(\gamma\frac{\breve{\omega}_n}{\sqrt{\bar{\alpha}_2}}\right)\sin(\gamma\breve{\omega}_n)\right.\right.\\&\left.\left.+\frac{\sqrt{\bar{\alpha}_2}}{\bar{k}_2}\cos\left(\gamma\frac{\breve{\omega}_n}{\sqrt{\bar{\alpha}_2}}\right)\cos(\gamma\breve{\omega}_n)\right)\cos\left(\frac{\breve{\omega}_n(\gamma+\xi_{LS,2b})}{\sqrt{\bar{\alpha}_2}}\right)\right]\exp\left(-\breve{\omega}_n^2(\tau-\tau_B^*)\right)\Bigg]\Bigg\}\end{aligned} \tag{70}$$

Stage C, and consequently Case II ends at $\tau=\tau_C^*$, when layer 2 is melted completely i.e., $\xi_{LS,2a}(\tau_C^*)+\xi_{LS,2b}(\tau_C^*)=1-\gamma$.

Note that depending on the values of various non-dimensional parameters that govern the relative rates of melting and temperature rise in the two layers, Stage C may or may not occur. Stage C occurs when temperature in layer 1 after melting rises sufficiently to cause a secondary melting front in layer 2 before it is fully melted. Given that sensible temperature rise in most materials occurs faster than the rate of phase change propagation due to the usually large value of the latent heat, therefore, it is likely that Stage C will occur in most practical scenarios with PCMs of realistic thermal properties.

The next section discusses key results, including comparison with numerical simulations, analysis of temperature fields and melting front

propagation based on the equations derived here, as well as the derivation of conditions for simultaneous completion of melting in both layers.

3. Results and discussion

3.1. Comparison with numerical simulations

A comparison of the theoretical model with numerical simulations is carried out first using a finite-element simulation code in ANSYS CFX. The numerical simulation is carried out by treating each PCM to be a heterogeneous binary mixture comprising the two phases, with independent thermal properties defined for both, as well as the phase change temperature and latent heat of phase change. The numerical simulation solves the enthalpy formulation of the energy conservation [16] over a discretized grid, wherein the latent heat of fusion is included within the definition of the enthalpy. Finally, the phase change front at a given time is determined manually by determining the location at which the temperature computed by the numerical simulation is equal to the phase change temperature. The element size and timestep for the simulations are chosen as 0.01 mm and 1 s. It is verified that further mesh size and timestep refinement do not result in significant changes in the temperature field. Accuracy of the simulations is established by ensuring good agreement with the analytical solution for the special case of one-dimensional melting in a single PCM due to a constant temperature wall.

Octadecane and eicosane, with thermal properties listed in Table 1 [33,34] are chosen as the PCMs for layers 1 and 2, respectively. Both layers have a length of 5 mm. Two specific scenarios are considered in terms of temperatures imposed on the two walls. In the first scenario, when the imposed temperatures on the left and right walls are 44 and 70 °C, melting is found to occur according to Case I discussed in Section 2.1. In the second scenario, Case II melting occurs when the imposed temperatures on the left and right walls are 44 and 50°C, respectively. For these two scenarios, comparison between the theoretical model and numerical simulations is presented in terms of locations of various phase change fronts as functions of time in Figs. 3 and 4, respectively. Values of various non-dimensional parameters based on dimensional parameters listed above are also indicated. Good agreement is observed in general for each melting front in each scenario. The mean relative errors for $\xi_{LS,1a}$, $\xi_{LS,1b}$ and $\xi_{LS,2a}$ in Case I (Fig. 3) are found to be 2.1%, 14.2% and 6.3%, respectively. The mean relative error for $\xi_{LS,1a}$, $\xi_{LS,1b}$, $\xi_{LS,2a}$ and $\xi_{LS,2b}$ in Case II (Fig. 4) are found to be 2.6%, 1.3%, 11.3% and 4.2%, While these error magnitudes are relatively small, the highest error is found to be for $\xi_{LS,2a}$, which is the the primary propagation front in the second PCM that is not described by an exact Stefan problem. The relatively small difference between the present work and simulations may be attributed to the approximate nature of the modeling technique used in this work, as well as possible discretization errors in the numerical simulations. The theoretical model developed in this work is based on approximating the temperature field in the melted region at any time with the solution of the transient energy conservation equation. As discussed in past work [7,8], even though this technique is expected to be more accurate than the quasi-steady approach, it is nevertheless an approximation. This, combined with potential errors involved in the numerical simulations, such as discretization errors, may explain the slight discrepancy between the theoretical model and

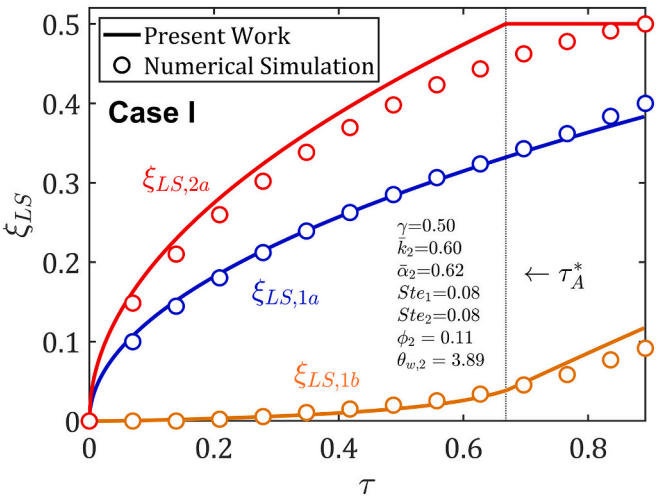

Fig. 3. Comparison between present analytical model and finite-element simulation: Phase change fronts in both layers as functions of time for a Case I scenario, in which layer 2 finishes melting first. Results from a finite-element simulation are presented for comparison.

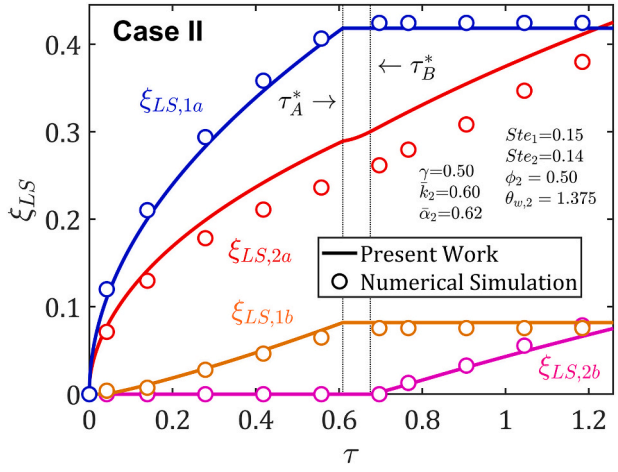

Fig. 4. Comparison between present analytical model and finite-element simulation: Phase change fronts in both layers as functions of time for a Case II scenario, in which layer 1 finishes melting first. Results from a finite-element simulation are presented for comparison.

numerical simulations observed in some of the curves in Figs. 3 and 4. One particular source of potential error from the numerical simulation is the approximate nature of the modeling of the melting process and the need for manual identification of the phase change front in the temperature field at a given time. Minimizing these sources of error may help obtain the best-possible agreement between the two, although an exact match is not expected due to the approximate nature of both techniques.

Table 1
Values of thermal properties of the two PCMs used in this work [33,34].

	Octadecane	Eicosane
Thermal conductivity, $Wm^{-1}\,K^{-1}$	0.25	0.15
Heat capacity, $Jkg^{-1}\,K^{-1}$	2300	2210
Density, kgm^{-3}	780	785
Latent heat, Jkg^{-1}	244,000	247,000
Phase change temperature, °C	28	36

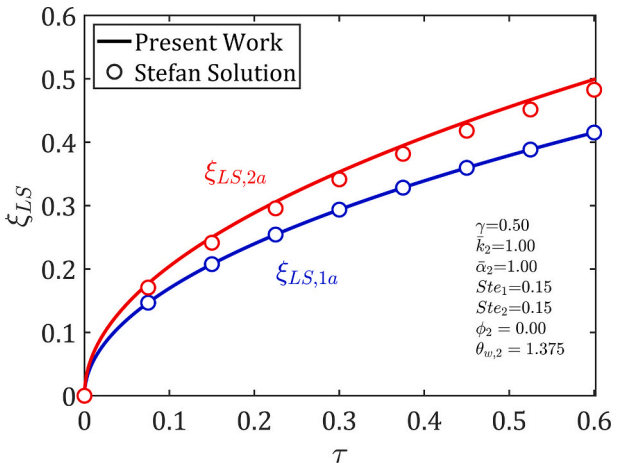

Fig. 5. Comparison between present analytical model and exact Stefan solution for a special case: Phase change fronts in both layers as functions of time for a scenario where both layers are made of the same PCM (octadecane). Non-dimensional parameter values are $\gamma = 0.50, \bar{k}_2 = 1, \bar{\alpha}_2 = 1, Ste_1 = 0.15, Ste_2 = 0.15, \phi_2 = 0, \theta_{w,2} = 1.375$. Results from the exact Stefan solution are also shown for comparison.

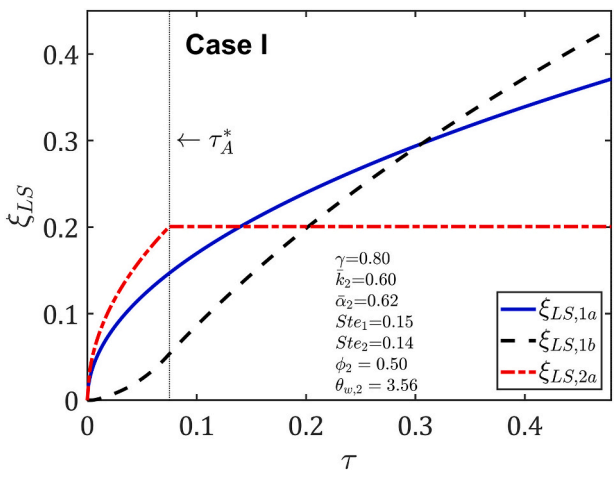

Fig. 6. Illustration of the melting process for Case I scenario: Phase change fronts in both layers as functions of time for a Case I scenario in which layer 2 finishes melting first. Parameter values are $\gamma = 0.80, Ste_1 = 0.15, Ste_2 = 0.14, \bar{\alpha}_2 = 0.62, \bar{k}_2 = 0.60, \phi_2 = 0.50, \theta_{w,2} = 3.56$.

3.2. Results for a special case

The theoretical model presented here accounts for two PCMs with distinct thermal properties and thicknesses arranged in series, along with two distinct wall temperatures imposed at the two ends. It is interesting to investigate the predictions of the theoretical model for a special case in which both PCMs are made of the same material. In such a scenario, two independent phase change fronts are expected to propagate inwards from both ends, both driven only by heat transfer from their respective walls. Each is expected to be governed by the exact analytical solution for the Stefan problem of one-dimensional phase change driven by a constant temperature wall [1,5]. Results from the theoretical model presented here for this special case are presented and compared against the analytical Stefan solution in Fig. 5 in terms of the locations of the two phase change propagation fronts as functions of time. Corresponding to 5 mm thickness of octadecane and eicosane each, and driven by wall temperatures of 44 and 50 °C, respectively, the non-dimensional problem parameters are $\gamma = 0.50, \bar{k}_2 = 1, \bar{\alpha}_2 = 1, Ste_1 = 0.15, Ste_2 = 0.15, \phi_2 = 0, \theta_{w,2} = 1.375$. Good agreement between the two-PCM theoretical model and the exact Stefan solution is observed for this special case, as expected. This shows that under specific conditions, the general two-PCM model presented in this work correctly reduces to the special case of a one-PCM problem, which is governed by the Stefan solution.

3.3. Typical melting front propagation plots

Fig. 6 presents a plot of the melting front locations as functions of time for a problem in which melting occurs according to the Case I scenario discussed in Section 2.1. Both primary and secondary melting fronts in layer 1, as well as the primary melting front in layer 2 are shown. The problem parameters are $\gamma = 0.80, Ste_1 = 0.15, Ste_2 = 0.14, \bar{\alpha}_2 = 0.62, \bar{k}_2 = 0.60, \phi_2 = 0.50, \theta_{w,2} = 3.56$. Fig. 6 clearly shows the propagation of each melting front over time. The two primary melting fronts $\xi_{LS,1a}$ and $\xi_{LS,2a}$ propagate rapidly at early times, due to immediate heat transfer from the left and right walls, respectively, followed by a slow down in the rate of propagation at later times, which is due to the well-known effect of growing thermal impedance offered by the melted regions as more and more material melts [1]. In contrast, the secondary melting front in layer 1, $\xi_{LS,1b}$, which starts from the inter-layer interface and propagates left-wards, starts slowly because in order for $\xi_{LS,1b}$ to grow, heat must first conduct through layer 2 before starting to melt layer 1. Once sufficient heat has conducted across layer 1, $\xi_{LS,1b}$ begins to grow more rapidly.

As shown in Fig. 6, Stage A finishes when layer 2 has finished melting, i.e., at $\tau = \tau_A^*$ when $\xi_{LS,2a} = 1 - \gamma$. Some of the factors that contribute towards the completion of melting in layer 2 first include its smaller size compared to layer 1 as well as the relatively larger temperature of the right wall. During Stage B ($\tau > \tau_A^*$), Fig. 6 shows a static location of $\xi_{LS,2a}$, while the two melting fronts in layer 1 continue to grow until their sum $\xi_{LS,1a} + \xi_{LS,1b}$ becomes equal to the thickness of layer 1, γ, at which time, layer 1 has also finished melting and the overall melting process is complete.

Fig. 7 presents similar melting propagation plots for Case II, in which layer 1 first finishes melting in Stage A. In contrast with $\gamma = 0.8$ assumed in Fig. 6, here, $\gamma = 0.5$, so that layer 1 is relatively thinner, which contributes towards the completion of melting first in layer 1, i.e., Case II. Fig. 7(a) represents a scenario in which layer 2 finishes melting by the end of Stage B, so that Stage C does not occur, whereas Fig. 7(b) represents a scenario in which Stage C occurs, as discussed in Section 2.2.3, mainly due to a relatively lower right wall temperature. Similar to Case I shown in Fig. 6, rapid rise in $\xi_{LS,1a}$ and $\xi_{LS,2a}$ at early times is also observed in this case. Similarly, the secondary melting fronts start slowly in both Figs. 7(a) and 7(b) due to the time taken for heat transfer through the other layer. Note that the secondary melting front in layer 2 is completely absent in Fig. 7(a) and begins only at the start of Stage C in Fig. 7(b), because only one primary melting front occurs in layer 2 during Stages A and B under the conditions assumed in this Figure.

Until the completion of Stage A, Figs. 6 and 7 are, in principle similar, because Stage A of both Cases differ only in terms of which layer finishes melting first. In Case II, layer 1 finishes melting first, as seen in the flat $\xi_{LS,1a}$ and $\xi_{LS,1b}$ curves beyond $\tau = \tau_A^*$ in both Figs. 7(a) and 7(b). Beyond $\tau = \tau_A^*$, $\xi_{LS,2a}$ continues to grow, representing continued melting of layer 2. The key difference between the scenarios shown in Figs. 7(a) and 7(b) is that in Fig. 7(a), all of layer 2 finishes melting due to the primary left-propagating melting front caused by the right wall, and there is no secondary melting front in layer 2 in this case. In contrast, Fig. 7(b) shows that after a brief Stage B, a secondary melting front $\xi_{LS,2b}$ is initiated and contributes towards further melting of layer 2. In this case, layer 2, and, therefore, the entire two-PCM stack finishes melting when the total sum of the two melting fronts in layer 2 equals layer 2 thickness, i.e., $\xi_{LS,2a} + \xi_{LS,2b} = 1 - \gamma$.

Note that the right wall melting temperatures for Figs. 7(a)(a) and 7

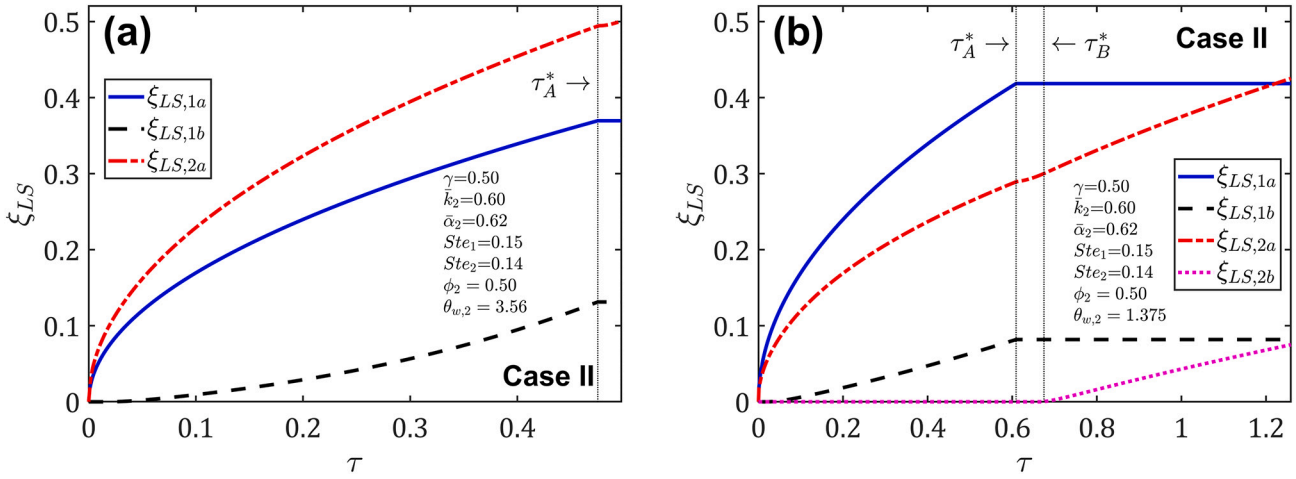

Fig. 7. Illustration of the melting process for Case II scenario: Phase change fronts in both layers as functions of time for a Case II scenario in which layer 1 finishes melting first. (a) $\theta_{w,2} = 1.375$ (Stage C does not occur), (b) $\theta_{w,2} = 3.56$ (Stage C occurs). Other parameter values are $\gamma = 0.50, Ste_1 = 0.15, Ste_2 = 0.14, \bar{\alpha}_2 = 0.62, \bar{k}_2 = 0.60, \phi_2 = 0.50$.

(b) are $\theta_{w,2} = 3.56$ and $\theta_{w,2} = 1.375$, respectively. The greater wall temperature for the case shown in Fig. 7(a) contributes towards the completion of melting of layer 2 during Stage B without the initiation of a second melting front in layer 2 (Stage C), in contrast with Fig. 7(b), where, due to the relatively lower value of $\theta_{w,2}$, the primary melting front in layer 2 propagates somewhat slower, resulting in a second melting front when the inter-layer interface temperature reaches the melting temperature of layer 2. These features are clearly seen in Figs. 7 (a) and 7(b).

3.4. Typical temperature distribution plots

In order to further illustrate the nature of the phase change problem, temperature distributions in both layers are computed at different times. Fig. 8 presents temperature distribution plots for Case I, with the same set of parameters as Fig. 6. The vertical and horizontal dotted lines indicate the inter-layer interface γ on the ξ axis, and the melting temperature of layer 2, ϕ_2, on the θ axis, respectively. Plots at the first three times correspond to Stage A, during which, both layers 1 and 2 melt.

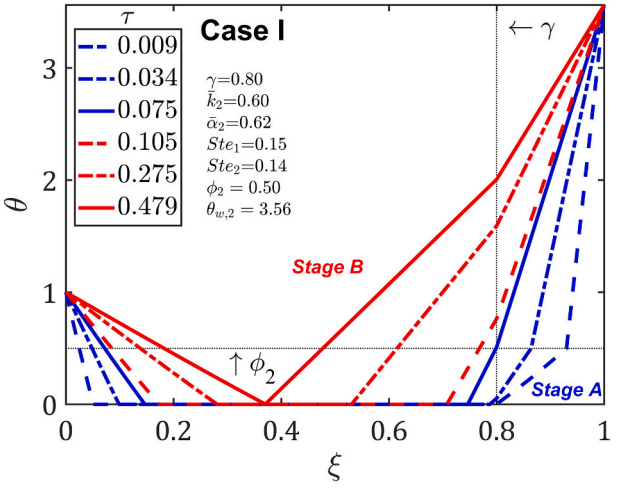

Fig. 8. Illustration of the melting process for Case I scenario: Temperature distributions at various times for a Case I scenario in which layer 2 finishes melting first. Parameter values are identical to Fig. 6.

Propagation of the melting fronts can be seen clearly in Fig. 8 through the inwards shift in temperature curves in both layers. In particular, the temperature curves in layer 1 shift inwards from both left and right, signifying the two simultaneous melting fronts in layer 1. Consistent with the definition of Case I, layer 2 finishes melting first, at around $\tau = 0.075$, when the temperature at the interface reaches ϕ_2, signifying that all of layer 2 has melted. Afterwards, there continues to be further sensible temperature rise in layer 2, whereas the two melting fronts in layer 1 continue to propagate inwards until meeting each other at around $\xi = 0.37$ at $\tau = 0.479$, signifying the final completion of the melting process. The times at which Stages A and B are found to finish in Fig. 8 are consistent with the phase change propagation plot for this Case presented in Fig. 6.

Similar temperature distributions at different times for Case II are presented in Fig. 9. Under the conditions assumed in Figs. 7(a) and 7(b), two distinct plots for scenarios in which Stage C does not occur or occurs are presented in Figs. 9(a) and 9(b), respectively. Fig. 9(a) shows simultaneous melting of layers 1 and 2, with both primary and secondary melting fronts in layer 1, similar to Fig. 8. The distinction between Figs. 9(a) and 8 is that in Fig. 9(a), the melting of layer 1 is completed first, as shown by the meeting of the two melting fronts at $\xi = 0.37$ at $\tau = 0.475$. In Fig. 9(a), Stage A is followed by the melting of the remainder of layer 2, along with sensible heating of melted regions in both layers. In this case, only a very small fraction of layer 2 undergoes melting in Stage B, due to which, the Stage B curves in layer 2 are nearly coincident.

In contrast, Fig. 9(b) presents temperature distributions for a scenario in which Stage B does not finish with complete melting of layer 2. Rather, at a certain time in Stage B, the temperature at the interface rises to the melting temperature of layer 2, which results in the initiation of a secondary melting front in layer 2, starting at the interface and moving rightwards as time passes, as shown by the Stage C curves in Fig. 9(b). Eventually, at the end of Stage C, the two inwards-propagating melting fronts in layer 2 meet each other at around $\xi = 0.57$, at which point, the entire melting process is complete.

Figs. 8 and 9 provide further insights into the temperature distributions in the two layers during the melting process. An investigation of parameters that characterize the overall melting process, and their dependence on key non-dimensional parameters is carried out next.

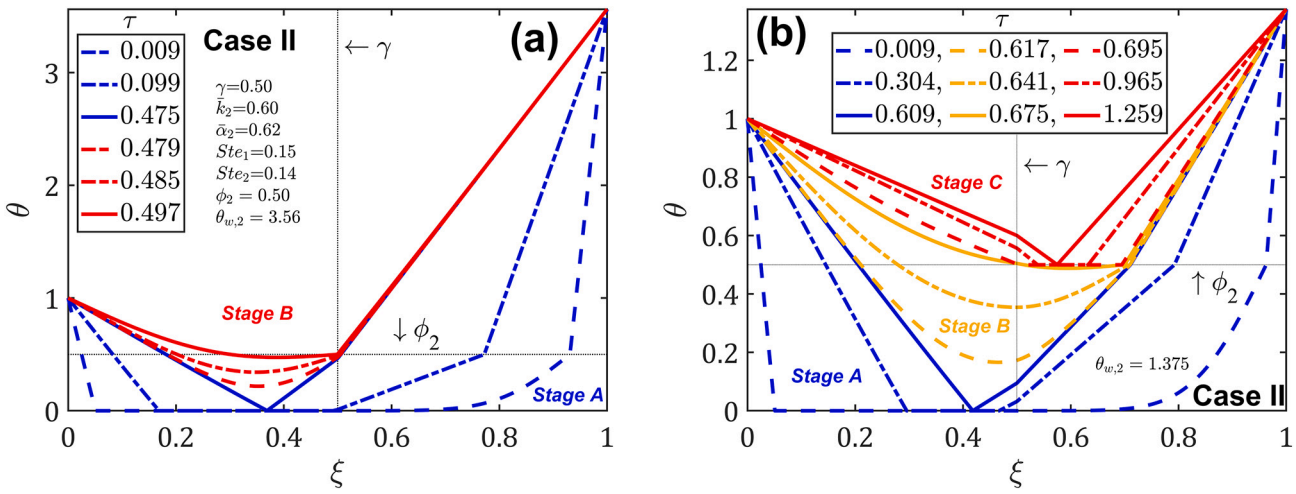

Fig. 9. Illustration of the melting process for Case II scenario: Temperature distributions at various times for a Case II scenario in which layer 1 finishes melting first. (a) and (b) present results for parameter values corresponding to Figs. 7(a) and 7(b), respectively.

3.5. Impact of Stefan numbers

Similar to other phase change problems, Stefan number is the key non-dimensional parameter that governs the propagation of the melting process in the present problem. Stefan number combines the imposed temperature difference with thermophysical properties of the PCM, namely, the heat capacity and latent heat. Due to the presence of two distinct PCMs, two different Stefan numbers, as defined in Section 2.2, appear in the present problem. Note that both Stefan numbers defined in this work are based on properties of the respective layers, but, for mathematical convenience, both use the temperature imposed at the left wall. The impact of the Stefan numbers on phase change propagation and on the total time to melt is investigated next.

Figs. 10(a) and 10(b) plot phase change front propagation as a function of time for three different values of Ste_1 and Ste_2, respectively. Other parameter values are $\gamma = 0.50, \bar{\alpha}_2 = 0.62, \bar{k}_2 = 0.60, \phi_2 = 0.50, \theta_{w,2} = 1.375$. Values of Ste_2 and Ste_1 for Figs. 10(a) and 10(b) are 0.14 and 0.15, respectively. In general, Figs. 10(a) and 10(b) show that as the Stefan number goes up, the rate at which melting propagates rises, as expected.

Fig. 10(a) shows greater rate of melting of both layers 1 and 2 with increasing Ste_1, although the total time to melt is largely independent of Ste_1. Fig. 10(a) also offers additional insights into the impact of Ste_1 on the melting rate at different stages. It shows that increasing the value of Ste_1 reduces the complete melting time of layer 1 in Stage A. However, it has no effect on the melting rate of layer 2 during this stage. In other words, the slope of $\xi_{LS,2}$ remains unchanged for different values of Ste_1 during Stage A. The reason behind this is that, during Stage A, as long as there is an unmelted region in layer 1, no heat diffusion occurs from the right wall to layer 2 to affect its melting rate. In other words, increasing the parameter Ste_1 shortens the melting time of layer 1 but not that of layer 2. Subsequently, sensible heating through layer 1 in stages B and C speed up the melting of layer 2.

In contrast with Fig. 10(a), Fig. 10(b) demonstrates that increasing the value of Ste_2 significantly decreases the melting rate of layer 2, while having only a minor effect on the melting rate of layer 1. This negligible effect can be attributed to the fact that Ste_2 only affects the melting rate of layer 1 from its right side through the secondary melting front $\xi_{LS,1b}$, which contributes only a small fraction of the total melted thickness of layer 1.

The time required for complete melting is an important performance parameter in practical energy storage systems. Figs. 11(a) and 11(b) investigate the impact of Ste_1 and Ste_2, respectively, on the total time taken for complete melting. Fig. 11(a) shows that increasing Ste_1 reduces the melting time of layer 1. This reduction is quite sharp for small values of Ste_1, and the curves becomes flatter for larger values. This may

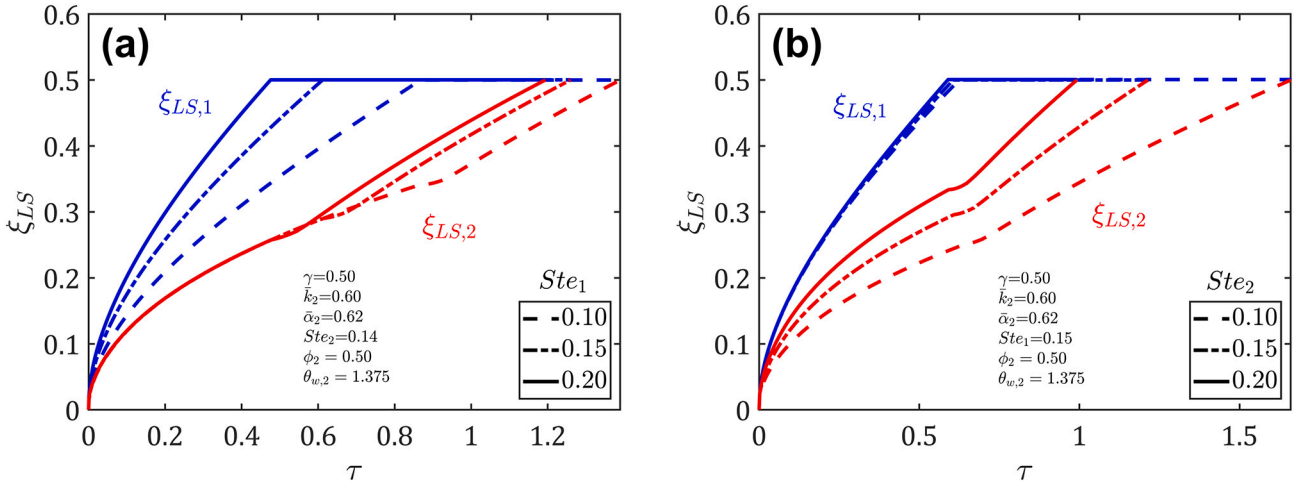

Fig. 10. Impact of Stefan numbers on melting propagation: Total melted thickness in each layer as a function of time for three different values of (a) Ste_1 (with $Ste_2 = 0.14$); b) Ste_2 (with $Ste_1 = 0.15$). Other parameter values in this Case II scenario are $\gamma = 0.50, \bar{\alpha}_2 = 0.62, \bar{k}_2 = 0.60, \phi_2 = 0.50, \theta_{w,2} = 1.375$.

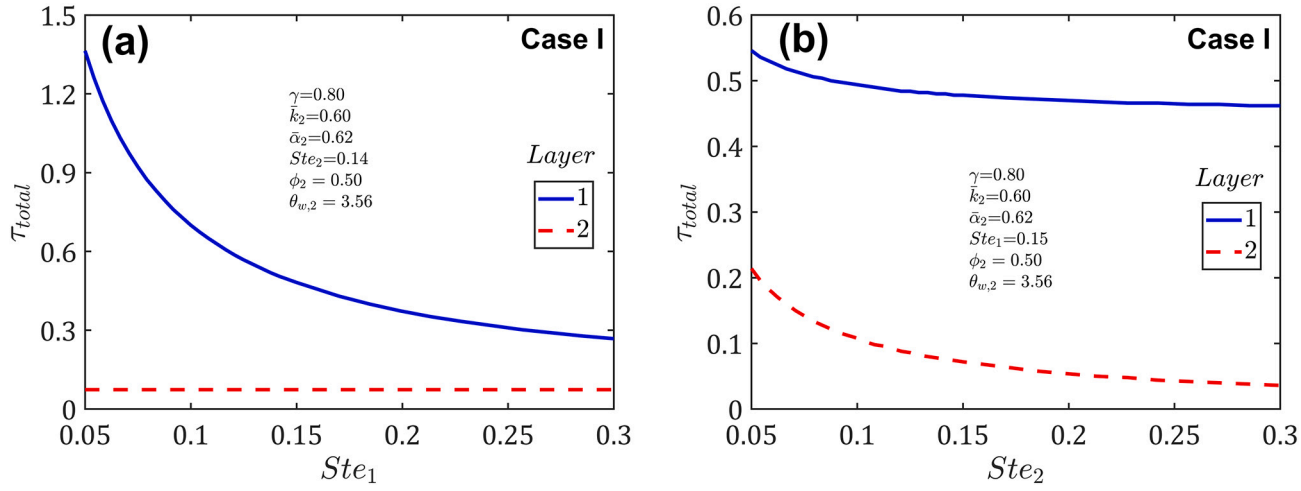

Fig. 11. Impact of Stefan numbers on melting propagation in a Case I scenario: Total time taken for complete melting of each layer as a function of (a) Ste_1 (with $Ste_2 = 0.14$); b) Ste_2 (with $Ste_1 = 0.15$). Other parameter values are $\gamma = 0.80, \bar{\alpha}_2 = 0.62, \bar{k}_2 = 0.60, \phi_2 = 0.50, \theta_{w,2} = 3.56$.

be because of thermal conduction within the material becoming the dominant thermal conduction process as melting becomes easier when Ste_1 increases. It is also found that Ste_1 has no impact on the melting time of layer 2. This is because in Case I considered in Fig. 11(a), layer 2 finishes melting first on the basis of only the primary melting front directly from the right wall. There is no heat diffusion from the left wall through layer 1 to cause melting of layer 2, and, therefore, the melting time of layer 2 is independent of Ste_1.

In contrast, Fig. 11(b) presents the impact of Ste_2 on the melting time. Note that Ste_2 comprises the heat capacity and latent heat of layer 2 material, and the left wall temperature. As expected, Fig. 11(b)shows that increasing the value of Ste_2 has a more significant impact on the melting of layer 2 than layer 1. Note that in Case I, some of layer 1 melts due to heat transfer from the right wall through layer 2, and, therefore, the properties of layer 2, captured in Ste_2 have some impact on the melting of layer 1. This is the reason why the melting time curve for layer 1 in Fig. 11(b) is not completely flat, unlike Fig. 11(a), which shows no impact whatsoever of Ste_1 on the melting time of layer 2.

The discussion above pertains to Case I melting. Under certain conditions, the melting process may occur via Case II, as discussed in Section 2.2. Results for this Case are discussed in Fig. 12, where the total melting time of both layers as a function of Ste_1 and Ste_2 are depicted in Figs. 12(a) and 12(b), respectively. Fig. 12(a) shows that Ste_1 now impacts the melting of both layers, although, as expected, the impact on the melting time of layer 1 is stronger than layer 2. This is because, as discussed in Fig. 10(a), increasing Ste_1 decreases the melting time of layer 1 in Stage A. In addition, the impact of Ste_1 on melting of layer 2 is explained on the basis of heat diffusion through layer 1 to layer 2 being responsible for the melting of a part of layer 2 after Stage A. Fig. 12(b) illustrates the impact of Ste_2 on the melting times of both layers. As expected, Ste_2 does not significantly influence melting in layer 1.

3.6. Simultaneous completion of melting in both layers

Past work on thermodynamics analysis [18–20] suggests that in a stack of more than one PCMs, the simultaneous completion of melting of each layer is favorable. Mainly, one layer finishing melting early results in under-utilization of the overall latent heat storage capability. Therefore, the two-PCM stack, in particular, the thicknesses of the two layers, should be designed in order to ensure that both layers finish melting as close to each other as possible.

Such an optimization may be carried out using the theoretical techniques developed in this work. Here, the scenarios of layers 2 and 1 finishing the melting process at the end of Stage A are considered separately in Sections 2.1 and 2.2, respectively. The intersecting case in which both layers finish melting simultaneously at the end of Stage A

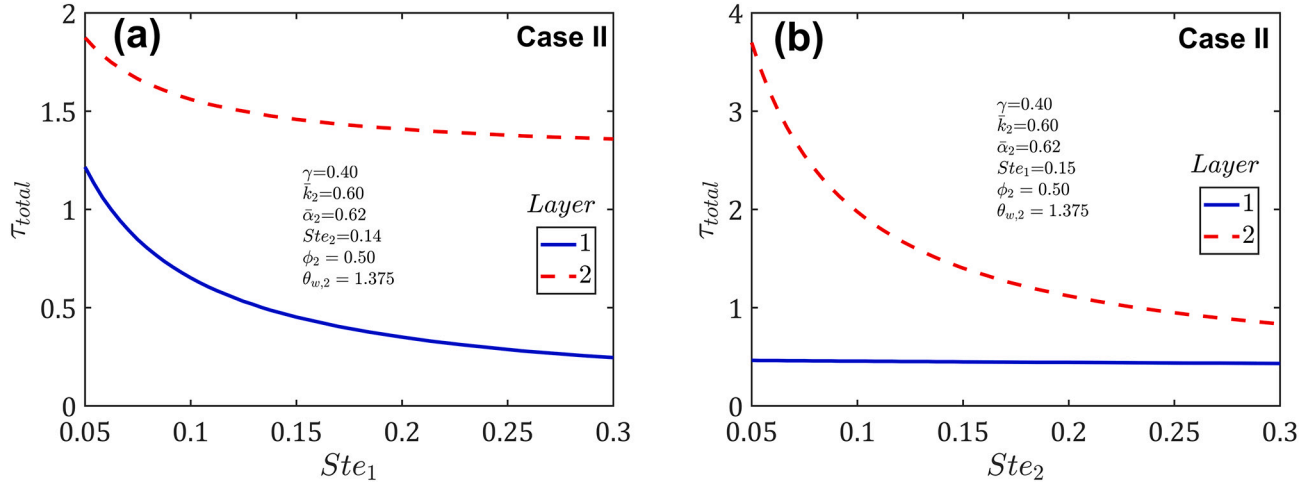

Fig. 12. Impact of Stefan numbers on melting propagation in a Case II scenario: Total time taken for complete melting of each layer as a function of (a) Ste_1 (with $Ste_2 = 0.14$); b) Ste_2 (with $Ste_1 = 0.15$). Other parameter values are $\gamma = 0.40, \bar{\alpha}_2 = 0.62, \bar{k}_2 = 0.60, \phi_2 = 0.50, \theta_{w,2} = 1.375$.

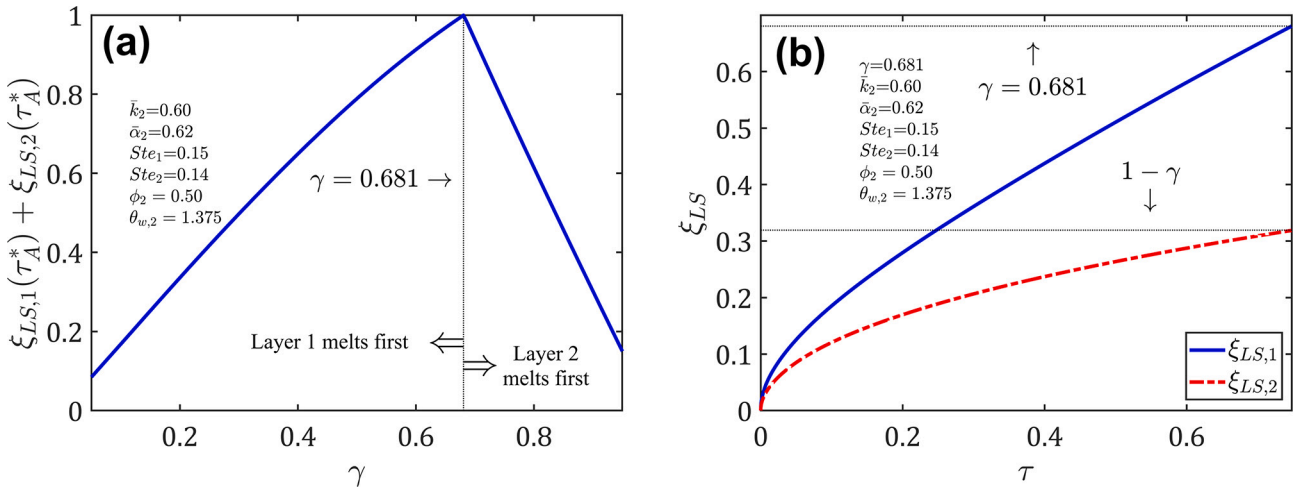

Fig. 13. Optimal layer thicknesses of simultaneous completion of melting in both layers: (a) Total material melted, $\xi_{LS,1} + \xi_{LS,2}$ at $\tau = \tau_A^*$ as a function of layer 1 thickness, γ. (b) Thickness of material melted in both layers as functions of time for the optimal value of layer 1 thickness, $\gamma = 0.681$. Other parameter values are $\gamma = 0.40, \bar{\alpha}_2 = 0.62, \bar{k}_2 = 0.60, \phi_2 = 0.50, \theta_{w,2} = 1.375$.

may be mathematically represented by the requirement that the total thickness of layers 1 and 2 melted, $\xi_{LS,1} + \xi_{LS,2}$ becomes equal to the thickness of the two-layer stack at $\tau = \tau_A^*$ in Case II. Note that $\xi_{LS,1}$ is the total thickness of layer 1 melted through both primary and secondary melting fronts, i.e., $\xi_{LS,1} = \xi_{LS,1,a} + \xi_{LS,1,b}$.

In principle, a number of non-dimensional parameters of this problem influence the relative rate of melting of the two layers. For example, while keeping other parameters constant, increasing or decreasing the relative thickness of layer 1, γ, is expected to increase or decrease the time of completion of melting of layer 1, respectively. At some intermediate value of γ, both layers may be expected to melt together. This is investigated in Fig. 13(a), which plots the total amount of materal melted at the end of Stage A, $\xi_{LS,1}(\tau_A^*) + \xi_{LS,2}(\tau_A^*)$ as a function of layer 1 thickness γ. As γ increases, more and more of the PCM stack melts by the end of Stage A, because layer 1 has the lower melting temperature of the two layers, and, therefore, greater fraction of layer 1, γ, results in greater total melting during Stage A. However, a maxima in the curve occurs at a certain layer 1 thickness, at which, both layers have finished melting by the end of Stage A. This is the largest possible amount of total melting, and further increase in γ beyond this value pushes the melting process into Case I, as shown in Fig. 13(a), implying that layer 2 thickness is sufficiently thin now that layer 2 finishes melting first, and much of layer 1 remains unmelted, which in an undesirable scenario. In between these extremes, an optimal value of $\gamma = 0.681$ obtained from Fig. 13(a) ensures simultaneous completion of melting of both layers by the end of Stage A.

The melting of both layers under these optimal conditions is further illustrated in Fig. 13(b), in which, the total thicknesses of layers 1 and 2 melted, $\xi_{LS,1}$ and $\xi_{LS,2}$, respectively, are plotted as functions of time at the optimal value of $\gamma = 0.681$. It is found that melting fronts in both layers propagate with time, and at the end of Stage A, $\tau = \tau_A^*$, the melted thicknesses of the two layers are 0.681 and 0.319, respectively, confirming that the entire PCM stack has melted.

While presented in the context of determining the optimal layer thickness to ensure simultaneous completion of melting in both layers, the theoretical model presented in this work can also be used to optimize other problem parameters, such as the two wall temperatures and thermal properties of the two materials in order to obtain the thermodynamically optimal scenario of melting in both layers finishing together.

4. Conclusions

The key novelty of the present work is that it provides a quantitative model for predicting the nature of phase change propagation when a stack of two PCMs is heated up from both sides. In contrast, past work mostly addressed scenarios with only a single PCM, and the limited work available on more than one PCMs either did not present an analytical model, or assumed that the PCM stack is being heated up only from one side. As the present work shows, several interesting scenarios occur in the case of two-sided melting, such as the existence of up to three simultaneous melting fronts.

The sequential or parallel melting of both layers, depending on the imposed conditions is systematically analyzed in this work, and the presence of two or more melting fronts is accounted for by determining the temperature distribution, and, subsequently, the rate of melting front propagation. While the technique is inherently approximate in nature, good accuracy may be expected for reasonably low values of the two Stefan numbers that appear in this problem.

A key quantitative contribution of the analysis presented here is in the identification of a theoretical condition that results in both PCMs finishing their respective melting processes simultaneously. Such a condition can be used to design thermodynamically optimal two-PCM stacks that maximize the capability of energy storage or thermal management. Since the analysis and key results are presented in non-dimensional term, this work may be readily used to analyze a wide variety of problems. For example, Fig. 13 shows that under the conditions considered, both layers finish melting simultaneously when the composite stack comprises 68.1% of the first layer.

While this work is discussed in the context of melting, it is equally applicable for the opposite process of solidification. Key approximations made in the present work include negligible change in thermal transport properties with temperature and negligible heat transfer due to buoyancy-driven natural convection. These are both reasonable approximations when the temperature rise in the problem is not very large, such as in thermal management of microelectronic devices. However, for other applications where much greater temperature change is encountered, such as in manufacturing based on melting of metals, it may become necessary to account for these effects, or, at least, estimate the errors involved in the approximations made in this work.

CRediT authorship contribution statement

Emad Hasrati: Formal analysis, Validation, Investigation, Data

curation, Writing – original draft, Writing – review & editing. **Ankur Jain:** Conceptualization, Methodology, Investigation, Project administration, Writing – original draft, Writing – review & editing.

Declaration of Competing Interest

The authors declare that they have no known competing financial interests or personal relationships that could have appeared to influence the work reported in this paper.

Data availability

Data will be made available on request.

References

[1] V. Alexiades, A.D. Solomon, Mathematical Modeling of Melting and Freezing Processes, CRC Press, 1993.
[2] R. Viskanta, Heat transfer during melting and Solidification of metals, J. Heat Transf. 110 (1988) 1205–1219, https://doi.org/10.1115/1.3250621.
[3] V.J. Lunardini, Heat Transfer with Freezing and Thawing, 1st ed., Elsevier Science, 1991.
[4] M. Parhizi, A. Jain, Analytical modeling and optimization of phase change thermal management of a Li-ion battery pack, Appl. Therm. Eng. 148 (2019) 229–237, https://doi.org/10.1016/j.applthermaleng.2018.11.017.
[5] J. Stefan, Über die Theorie der Eisbildung, insbesondere über die Eisbildung im Polarmeere, Ann. Phys. 278 (2) (1891) 269–286.
[6] G.S. Cole, Transport processes and fluid flow in solidification, in: T.J. Hugel, G. F. Bolling (Eds.), Solidification, AIME Publishing, 1969, pp. 201–274.
[7] M. Parhizi, A. Jain, Theoretical modeling of solid-liquid phase change in a phase change material protected by a multilayer Cartesian wall, Int. J. Heat Mass Transf. 197 (2022) 123330, 1–16, https://doi.org/10.1016/j.ijheatmasstransfer.2022.123330.
[8] A. Jain, M. Parhizi, Theoretical analysis of phase change heat transfer and energy storage in a spherical phase change material with encapsulation, Int. J. Heat Mass Transf. 185 (2022) 122348, 1–12, https://doi.org/10.1016/j.ijheatmasstransfer.2021.122348.
[9] D.L.R. Oliver, J.E. Sunderland, A phase change problem with temperature-dependent thermal conductivity and specific heat, Int. J. Heat Mass Transf. 30 (1987) 2657–2661, https://doi.org/10.1016/0017-9310(87)90147-5.
[10] M. Parhizi, A. Jain, Solution of the phase change Stefan problem with time-dependent heat flux using perturbation method, J. Heat Transf. 141 (2019) 024503, 1–5, https://doi.org/10.1115/1.4041956.
[11] J. Caldwell, Y.Y. Kwan, On the perturbation method for the Stefan problem with time-dependent boundary conditions, Int. J. Heat Mass Transf. 46 (2003) 1497–1501, https://doi.org/10.1016/S0017-9310(02)00415-5.
[12] R. Goodman, The heat-balance integral—further considerations and refinements, J. Heat Transf. 83 (1961) 83–85, https://doi.org/10.1115/1.3680474.
[13] D. McCord, J. Crepeau, A. Siahpush, J.A.F. Brogin, Analytical solutions to the Stefan problem with internal heat generation, Appl. Therm. Eng. 103 (2016) 443–451, https://doi.org/10.1016/j.applthermaleng.2016.03.122.
[14] G. Krishnan, M. Parhizi, A. Jain, Eigenfunction-based solution for solid-liquid phase change heat transfer problems with time-dependent boundary conditions, Int. J. Heat Mass Transf. 189 (2022) 122693, 1–12, https://doi.org/10.1016/j.ijheatmasstransfer.2022.122693.
[15] A. Barba, M. Spiga, Discharge mode for encapsulated PCMs in storage tanks, Sol. Energy 74 (2003) 141–148, https://doi.org/10.1016/S0038-092X(03)00117-8.
[16] A. Mori, K. Araki, Methods for analysis of moving boundary-surface problem, Int. Chem. Eng. 16 (1976) 734–744.
[17] D.W. Hahn, M.N. Özişik, Heat Conduction, Wiley, New York, 2012.
[18] J. Lim, A. Bejan, J. Kim, Thermodynamic optimization of phase-change energy storage using two or more materials, J. Energy Resour. Technol. 114 (1992) 84–90, https://doi.org/10.1115/1.2905925.
[19] T. Kousksou, F. Strub, J. Lasvignottes, A. Jamil, J. Bédécarrats, Second law analysis of latent thermal storage for solar system, Sol. Energy Mater. Sol. Cells 91 (2007) 1275–1281, https://doi.org/10.1016/j.solmat.2007.04.029.
[20] Z.X. Gong, A.S. Mujumdar, Finite element analysis of a multistage latent heat thermal storage system, Numer. Heat Trans. Part A 30 (1996) 669–684.
[21] R. Domański, G. Fellah, Exergy analysis for the evaluation of a thermal storage system employing PCMS with different melting temperatures, Appl. Thermal Eng. 16 (1996) 907–919, https://doi.org/10.1016/1359-4311(96)00003-8.
[22] M. Ezra, Y. Kozak, V. Dubovsky, G. Ziskind, Analysis and optimization of melting temperature span for a multiple-PCM latent heat thermal energy storage unit, Appl. Thermal Eng. 93 (2016) 315–329, https://doi.org/10.1016/j.applthermaleng.2015.09.040.
[23] M.M. Farid, Y. Kim, A. Kanzawa, Thermal performance of a heat storage module using PCM's with different melting temperature: mathematical modeling, J. Sol. Energy Eng. 111 (1989) 152–157, https://doi.org/10.1115/1.3268301.
[24] O.S. Elsanusi, E.C. Nsofor, Melting of multiple PCMs with different arrangements inside a heat exchanger for energy storage, Appl. Thermal Eng. 185 (2021) 116046, 1–10, https://doi.org/10.1016/j.applthermaleng.2020.116046.
[25] J. Wang, G. Chen, F. Zheng, Study on phase change temperature distributions of composite PCMs in thermal energy storage systems, Int. J. Energy Res. 23 (1999) 277–285, https://doi.org/10.1002/(SICI)1099-114X(19990325)23:4<277::AID-ER475>3.0.CO;2-Q.
[26] S. Shaikh, K. Lafdi, Effect of multiple phase change materials (PCMs) slab configurations on thermal energy storage, Energy Conv. Manag. 47 (2006) 2103–2117, https://doi.org/10.1016/j.enconman.2005.12.012.
[27] W. Li, J. Wang, X. Zhang, X. Liu, H. Dong, Experimental and numerical investigation of the melting process and heat transfer characteristics of multiple phase change materials, Int. J. Energy Res. 44 (2020) 11219–11232, https://doi.org/10.1002/er.5718.
[28] J. Wang, Y. Ouyang, G. Chen, Experimental study on charging processes of a cylindrical heat storage capsule employing multiple-phase-change materials, Int. J. Energy Res. 25 (2001) 439–447, https://doi.org/10.1002/er.695.
[29] H. Michels, R. Pitz-Paal, Cascaded latent heat storage for parabolic trough solar power plants, Sol. Energy 81 (2007) 829–837, https://doi.org/10.1016/j.solener.2006.09.008.
[30] S. Shaikh, K. Lafdi, C/C composite, carbon nanotube and paraffin wax hybrid systems for the thermal control of pulsed power in electronics, Carbon 48 (2010) 813–824, https://doi.org/10.1016/j.carbon.2009.10.034.
[31] T. Watanabe, H. Kikuchi, A. Kanzawa, Enhancement of charging and discharging rates in a latent heat storage system by use of PCM with different melting temperatures, Heat Recovery Syst. & CHP 13 (1993) 57–66, https://doi.org/10.1016/0890-4332(93)90025-Q.
[32] E. Hasrati, G. Krishnan, A. Jain, Freezing/melting in a composite wall comprising two distinct phase change materials in series, Int. J. Heat Mass Transf. (2023), https://doi.org/10.1016/j.ijheatmasstransfer.2023.125055 in press.
[33] D.V. Hale, M.J. Hoover, M.J. ONeill, Phase Change Materials Handbook. No. NASA-CR-61363, 1971.
[34] S. Himran, A. Suwono, G.A. Mansoori, Characterization of alkanes and paraffin waxes for application as phase change energy storage medium, Energy Sources 16 (1994) 117–128, https://doi.org/10.1080/00908319408909065.